Notes on simulating core collapse in massive scalar-tensor theories

December 10, 2023

Contents

1 Units

We will use units where the speed of light c, the gravitational constant G and the reduced Planck constant $\hbar$ are set to unity. In SI and cgs units, these constants are given by

$$\begin{aligned} c &= 2.99792458 \times 10^8 \,\frac{\mathrm{m}}{\mathrm{s}} = 2.99792458 \times 10^{10} \,\frac{\mathrm{cm}}{\mathrm{s}}\,, \\ G &= = 6.67408 \times 10^{-11} \,\frac{\mathrm{m}^3}{\mathrm{kg\,s}^2} = 6.67408 \times 10^{-8} \,\frac{\mathrm{cm}^3}{\mathrm{g\,s}^2}\,, \\ \hbar &= 1.054571800 \times 10^{-34} \,\frac{\mathrm{m}^2\,\mathrm{kg}}{\mathrm{s}} = 1.054571800 \times 10^{-27} \,\frac{\mathrm{cm}^2\,\mathrm{g}}{\mathrm{s}}\,. \end{aligned} \tag{1.1}$$

Some straightforward conventions we derive from this are

$$\begin{aligned} 1\,\mathrm{m} \text{ in } \mathrm{kg} &= 1.346635310 \times 10^{27}\,, \\ 1\,\mathrm{m}^{-1} \text{ in } \mathrm{kg} &= 3.517672883 \times 10^{-43}\,. \end{aligned} \tag{1.2}$$

The former relation uses $c = G = 1$ while the latter uses $c = \hbar = 1$. The latter relation implies in words that an inverse Compton wavelength of $1\,\mathrm{m}^{-1}$ corresponds to a particle with mass of $\sim 10^{-43}\,\mathrm{kg}$.

1.1 Astrophysical unit conversion

In astrophysics, cgs units are the most common choice. In our codes, we typically measure quantities in units of km, and we list here the most important conversion relations. Let us first recap briefly the most common cgs units,

$$\begin{aligned} 1\,\mathrm{m} &= 10^2\,\mathrm{cm}\,, \qquad 1\,\mathrm{kg} = 10^3\,\mathrm{g}\,, \\ 1\,\mathrm{dyn} &= 1\,\frac{\mathrm{g\,cm}}{\mathrm{s}^2} = 10^{-5}\,\frac{\mathrm{kg\,m}}{\mathrm{s}^2} = 10^{-5}\,\mathrm{N}\,. \end{aligned} \tag{1.3}$$

The most common conversions we need is for energy density and pressure into km based units or vice versa. The conversion factors are

$$\begin{aligned} 1\,\mathrm{km}^{-2} \text{ in } \mathrm{g\,cm}^{-3} &= 10^{-10}\,\frac{c^2}{G} = 1.34663530964 \times 10^{18}\,, \\ 1\,\mathrm{km}^{-2} \text{ in } \mathrm{dyn\,cm}^{-2} &= 10^{-10}\,\frac{c^4}{G} = 1.2102954584 \times 10^{39}\,. \end{aligned} \tag{1.4}$$

1.2 Particle physics conversion

Following Eq. (1.2), we noted that an inverse Compton wavelength corresponds to a particle of mass $\sim 10^{-43}\,\mathrm{kg}$. This may sound a very light particle, but we better measure particle masses in eV which requires yet one more conversion. We recall

$$1\,\mathrm{eV} = 1.602176565 \times 10^{-19}\,\mathrm{J}\,, \qquad 1\,\mathrm{J} = 1\,\frac{\mathrm{kg\,m^2}}{\mathrm{s^2}}\,, \tag{1.5}$$

so that

$$1\,\mathrm{m^{-1}}\ \text{in eV} = 1.973269788 \times 10^{-7}\,. \tag{1.6}$$

This is indeed light compared with a proton or electron, but we may actually be dealing with significantly lighter particles in our studies which then have a correspondingly larger Compton wavelength. For convenience, we rewrite the last relation in the form

$$\begin{aligned} 1\,\mathrm{eV}\ \text{in J} &= \frac{\mathrm{J}}{\mathrm{eV}} = 1.602176565 \times 10^{-19}\,, \\ 1\,\mathrm{eV}\ \text{in m}^{-1} &= \frac{(\mathrm{J/eV})}{c\,\hbar} = 5.067730759 \times 10^{6}\,, \\ 1\,\mathrm{eV^{-1}}\ \text{in m} &= 1.973269788 \times 10^{-7}\,. \end{aligned} \tag{1.7}$$

In order to get some idea of the values involved inour studies, we note that [11] find scalar fields with masses in the range $10^{-15}\,\mathrm{eV} \lesssim m_\varphi \lesssim 10^{-9}\,\mathrm{eV}$ are compatible with current observational constraints and may still produce significant scalarization effects. This translates, according to our unit conversion, to Compton wavelengths $\lambda\!\!\!^{-} := \hbar/(m_\varphi c)$ of about

$$10^{8}\,\mathrm{m} \gtrsim \lambda\!\!\!^{-}_\varphi \gtrsim 10^{2}\,\mathrm{m}\,. \tag{1.8}$$

We can also translate this into characteristic frequencies $f_\varphi = c/(2\pi\lambda\!\!\!^{-}_\varphi)$,

$$1\,\mathrm{Hz} \lesssim f_\varphi \lesssim 10^{6}\,\mathrm{Hz}\,. \tag{1.9}$$

This will become important later, as we will see that this characteristic frequency determines which part of the radiation spectrum is damped exponentially due to the non-zero mass of the scalar field: radiation modes with $f \lesssim f_\varphi$ decay exponentially with distance while the high-frequency modes propagate without energy loss. LIGO's sensitivity regime roughly spans $10\,\mathrm{Hz} \ldots 10^3\,\mathrm{Hz}$, so that it is sensitive to radiation of a massive scalar field only up to masses of the order of $m_\varphi \lesssim 10^{-11}\,\mathrm{eV}$. For higher masses, the modes LIGO could see are exponentially damped and never get far away from the source.

2 The field equations

Scalar-tensor theories of gravity are conveneniently formulated in either the physical or *Jordan-Fierz* frame or in the conformal or *Einstein* frame. We distinguish between quantities in these two frames by putting a bar on the Einstein variables while the Jordan variables remain unmarked.

2.1 The Jordan-Fierz frame

Starting point is the action given in the Jordan frame by

$$S = \int dx^4\sqrt{-g}\left[\frac{F(\phi)}{16\pi G}R - \frac{1}{2}g^{\mu\nu}(\partial_\mu\phi)(\partial_\nu\phi) - V(\phi)\right] + S_m(\psi_m, g_{\mu\nu}). \tag{2.1}$$

Here, the ψ_m collectively denote any matter fields that may be present in the spacetime. Note that these fields couple to the Jordan metric $g_{\mu\nu}$. We have two free function in this formalism, $F(\phi)$ and the potential $V(\phi)$. One may also introduce a third function $Z(\phi)$ as a factor in the middle term inside the brackets [1], but this function can be absorbed in the redefinition of the scalar field (2.11) leaving the field equation in the Einstein frame unchanged. This third function therefore does not introduce new physics and can be set to unity without loss of generality [US: Not 100 % certain here. I do not see any way, $Z(\phi)$ can introduce new physics, but just maybe I am overlooking something...] .
Varying the action (2.1) leads to the field equations

$$G_{\alpha\beta} = \frac{8\pi}{F}\left(T^F_{\alpha\beta} + T^\phi_{\alpha\beta} + T_{\alpha\beta}\right), \tag{2.2}$$

$$T^F_{\alpha\beta} = \frac{1}{8\pi}(\nabla_\alpha\nabla_\beta F - g_{\alpha\beta}\nabla^\mu\nabla_\mu F), \tag{2.3}$$

$$T^\phi_{\alpha\beta} = \partial_\alpha\phi\partial_\beta\phi - g_{\alpha\beta}\left[\frac{1}{2}g^{\mu\nu}\partial_\mu\phi\partial_\nu\phi + V(\phi)\right], \tag{2.4}$$

$$\Box\phi = -\frac{1}{16\pi}F_{,\phi}R + V_{,\phi}\,, \tag{2.5}$$

$$\nabla_\mu T^{\mu\alpha} = 0\,. \tag{2.6}$$

Here, the energy momentum tensor is defined as

$$T^{\alpha\beta} := \frac{2}{\sqrt{-g}}\frac{\delta S_m}{\delta g_{\alpha\beta}}\,, \tag{2.7}$$

and obeys the standard conservation equation (2.6) because it is coupled to the physical metric used in the Jordan frame.

2.2 The Einstein frame

We first recall that under a conformal transformation

$$g_{\mu\nu} \to \tilde{g}_{\mu\nu}\,, \tag{2.8}$$

the Ricci scalar transforms as

$$\tilde{R} = \Omega^{-2}\left[R - \frac{12\Box\sqrt{\Omega}}{\sqrt{\Omega}} + \frac{3}{\Omega^2}g^{\alpha\beta}(\nabla_\alpha\Omega)(\nabla_\beta\Omega)\right]. \tag{2.9}$$

An equivalent formulation of the scalar-tensor theory is then obtained by conformally transforming the metric according to

$$g_{\mu\nu} = \frac{1}{F(\phi)}\bar{g}_{\mu\nu} \qquad \Leftrightarrow \qquad \bar{g}_{\mu\nu} = F(\phi)\, g_{\mu\nu}\,, \tag{2.10}$$

and furthermore identifying the variables (see e.g. [13, 14])

$$\frac{\partial\varphi}{\partial\phi} = \sqrt{\frac{3}{4}\frac{F_{,\phi}{}^2}{F^2} + \frac{4\pi}{F}}\,, \qquad \Leftrightarrow \qquad \frac{\partial\phi}{\partial\varphi} = \sqrt{\frac{4F^2 - 3F_{,\varphi}{}^2}{16\pi F}}.\,, \tag{2.11}$$

$$V(\phi) = \frac{F^2}{4\pi}W(\varphi)\,. \tag{2.12}$$

The action (2.1) can then be rewritten in the form

$$\bar{S} = \frac{S}{F^2} = \frac{1}{16\pi G}\int dx^4\sqrt{-\bar{g}}\left[\bar{R} - 2\bar{g}^{\mu\nu}(\partial_\mu\varphi)(\partial_\nu\varphi) - 4W(\varphi)\right] + S_m[\psi_m, F^{-1}\bar{g}_{\mu\nu}]\,. \tag{2.13}$$

Note that the scalar field is now minimally coupled to the metric $\bar{g}_{\mu\nu}$, but the price for that simplification is that the non-gravitational matter fields couple to a conformally rescaled version of the metric used in the Einstein frame. Accordingly, the field equations for the metric simplify while the matter evolution is now more complex. The energy momentum tensor of the Einstein frame is defined as

$$\bar{T}^{\alpha\beta} := \frac{2}{\sqrt{-\bar{g}}}\frac{\delta S_m}{\delta\bar{g}_{\alpha\beta}} = F^{-3}(\varphi)\frac{2}{\sqrt{-g}}\frac{\delta S_m}{\delta g_{\alpha\beta}} = F^{-3}(\varphi)T^{\alpha\beta}\,. \tag{2.14}$$

and the field equations obtained from varying the action (2.13) are

$$\bar{G}_{\alpha\beta} = 2\partial_\alpha\varphi\partial_\beta\varphi - \bar{g}_{\alpha\beta}\bar{g}^{\mu\nu}\partial_\mu\varphi\partial_\nu\varphi + 8\pi\bar{T}_{\alpha\beta} - 2W(\varphi)\bar{g}_{\mu\nu}\,, \tag{2.15}$$

$$\bar{\Box}\varphi = 2\pi\frac{F_\varphi}{F}\bar{T} + W_{,\varphi}\,, \tag{2.16}$$

$$\bar{\nabla}_\mu\bar{T}^{\mu\alpha} = -\frac{1}{2}\frac{F_{,\varphi}}{F}\,\bar{T}\,\bar{g}^{\alpha\mu}\bar{\nabla}_\mu\varphi. \tag{2.17}$$

We finally note that in the literature, the conformal transformation is often alternatively written in terms of a function $a(\varphi)$ related to our F by $F = a^{-2}$. Also, sometimes convenient to use the logarithmic derivative

$$\alpha(\varphi) := \frac{a_{,\varphi}}{a} = -\frac{1}{2}\frac{F_{,\varphi}}{F}\,. \tag{2.18}$$

Most studies of scalar-tensor theory have considered conformal factors of the shape

$$\begin{aligned} & a(\varphi) = e^{\alpha_0(\varphi-\varphi_0)+\beta_0(\varphi-\varphi_0)^2}\,, \\ \Rightarrow\quad & F(\varphi) = e^{-2\alpha_0(\varphi-\varphi_0)-2\beta_0(\varphi-\varphi_0)^2}\,, \\ \Rightarrow\quad & \alpha(\varphi) = \alpha_0 + 2\beta_0(\varphi-\varphi_0)\,. \end{aligned} \tag{2.19}$$

With this form, we recover, in particular, that

$$\alpha_0 = \alpha(\varphi_0), \tag{2.20}$$

$$\beta_0 = \frac{\partial\alpha}{\partial\varphi}(\varphi_0), \tag{2.21}$$

and these are related to the Eddington parameters $\gamma_{\rm Edd}$, $\beta_{\rm Edd}$ by

$$\gamma_{\rm Edd} - 1 = \frac{-2\alpha_0^2}{1+\alpha_0^2}, \tag{2.22}$$

$$\beta_{\rm Edd} - 1 = \frac{\beta_0 \alpha_0^2}{2(1+\alpha_0^2)^2}. \tag{2.23}$$

For more details, see [4].

3 The matter fields

3.1 Primitive variables

We perform the matter evolution in the Jordan frame because that way we can effectively leave the shock capturing algorithm of GR1D [10] in place with only minor alterations of the flux and source terms and a tighter constraint on the time step due to the Courant-Friedrichs-Lewy stability condition; cf. [5] for details. The shock capturing technique requires the use of *conserved* variables for the matter fields. We will discuss these in the next subsection, but first formulate the matter content in terms of the more common *primitive* variables.
We model the stellar matter as a perfect fluid and write the energy momentum tensor in terms of the baryon density ρ, the pressure P, the enthalpy h and the four velocity u^α as

$$T_{\alpha\beta} = \rho h\, u_\alpha u_\beta + P g_{\alpha\beta}\,. \tag{3.1}$$

The enthalpy h is related to the specific internal energy ϵ by

$$h = 1 + \epsilon + \frac{P}{\rho} \qquad \Rightarrow \qquad \rho h = \rho(1+\epsilon) + P\,. \tag{3.2}$$

This amounts to three variables for the thermodynamic properties of the matter, baryon density ρ, pressure P and internal energy ϵ. In the static case, the latter two are determined from the baryon density through an equation of state which we will discuss further below. In the time dependent case, we actually have one further evolution equation that determines the change of the internal energy. For smooth evolutions, this time evolution can be shown to preserve the expression we use from the equation of state (by virtue of the first law of thermodynamics). In the presence of discontinuities, however, the internal energy may depart from that smooth evolution and we allow it in this case to provide an additional *thermal* pressure contribution.
In spherical symmetry, we write the line element

$$ds^2 = g_{\alpha\beta} dx^\alpha dx^\beta = -\alpha^2 dt^2 + X^2 dr^2 + \frac{r^2}{F} d\Omega^2\,, \tag{3.3}$$

where $d\Omega^2$ denotes the line element on the unit 2 sphere. Note that we specify the radial gauge in the Einstein frame. The matter can only move radially in this symmetry, so that the four velocity is determined by one function v which we define through

$$u^\alpha = \frac{1}{\sqrt{1-v^2}} \left[\frac{1}{\alpha}\,,\ \frac{v}{X}\,,\ 0\,,\ 0 \right]. \tag{3.4}$$

Note that the four velocity is normalized to $u_\mu u^\mu = -1$ with this definition and the our variable v can be written as

$$v = \frac{X}{\alpha}\frac{u^r}{u^t}\,. \tag{3.5}$$

In the literature, one often finds the alternative formulation of the energy momentum tensor in terms of the total energy density and the pressure. Novak [8, 7] uses such a notation and we conclude this subsection with identifying the relation between his and our variables. Novak writes

$$\begin{aligned} T_{\alpha\beta} &= (e+P)u_\alpha u_\beta + P g_{\alpha\beta}\,, \\ \Rightarrow \quad e &= \rho(1+\epsilon) = \rho h - P\,. \end{aligned} \tag{3.6}$$

Again, an equation of state is required to determine two variables as functions of the baryon density ρ: the pressure P and the total energy density e. Novak's notation for the four velocity is a bit more complicated, since he uses the four-velocity in the Einstein frame and rescales the velocity function with his metric components g_{rr} and g_{tt}. Ultimately, his and our notation are equivalent, but care needs to be taken when comparing results to make sure they correspond to the same frame, Einstein or Jordan.

3.2 Conserved variables

A flux conservative version of the matter sector of the field equations in spherical symmetry can be obtained by replacing the primitive variables ρ, h (or ϵ) and v with

$$\bar{D} = \frac{\rho X}{F\sqrt{F}\sqrt{1-v^2}}\,, \tag{3.7}$$

$$\bar{S}^r = \frac{\rho h v}{F^2(1-v^2)}\,, \tag{3.8}$$

$$\bar{\tau} = \frac{\rho h}{F^2(1-v^2)} - \frac{P}{F^2} - \bar{D}\,. \tag{3.9}$$

In the numerical evolution we need to constantly switch back and forth between the primitve and conservative variables. The step from the former to the latter is straightofrwardly done using the above Eqs. (3.7)-(3.9), but the reverse process is more involved because of the presence of the pressure P in the relations and its dependence on the baryon density ρ. In practice, the primitive variables are obtained from the conservative ones through an iterative process detailed in Sec. 4.1 of [5].

3.3 Equation of state

For most purposes, we use polytropic or piecewise polytropic equations of state. The latter have been found to provide good approximations to realistic equations of state; see [12] for tabulated parameters for a wide range of realistic equations of state.

We state here merely the expressions for a single polytrope; the extension to piecewise polytropic equations of state follows from continuity of the pressure. Note, however, that constants of integration must be inserted for the specific internal energy to ensure that ϵ is also a continuous function of ρ for the same polytropic parameters that make the pressure $P(\rho)$ a smooth function. As we mentioned

above, we have a time evolution equation for the specific internal energy. The equation of state therefore determines only a *cold* contribution of the internal energy which, however, coincides with that predicted by the time evolution equation provided no shocks have formed. In analogy, we also refer to the pressure predicted by the equation of state as the cold pressure. They are given by

$$P_c = K\rho^\Gamma\,, \tag{3.10}$$

$$\epsilon_c = \frac{K}{\Gamma-1}\rho^{\Gamma-1} = \frac{P_c}{(\Gamma-1)\rho}\,. \tag{3.11}$$

Note that the latter equation for the *cold* part of the specific internal energy follows from the first law of thermodynamics according to (recall $e = \rho + \rho\epsilon$ and that $\rho^{-1} \propto V$ where V is the volume)

$$\begin{aligned} & d\frac{\epsilon}{\rho} = -Pd\frac{1}{\rho} \\ \Rightarrow\quad & \epsilon = \int d\epsilon = -K\int \rho^\Gamma d\frac{1}{\rho} = -K\int v^{-\Gamma}dv = -K\frac{-1}{\Gamma-1}v^{-\Gamma+1} = \frac{K}{\Gamma-1}\rho^{\Gamma-1} = \frac{P}{(\Gamma-1)\rho} \end{aligned} \tag{3.12}$$

We assume here that the rest mass of the baryons ρ is not affected by thermodynamical processes (these change the energy contained in the interaction of the baryons but not the rest mass contained in a single baryon).
In the time evolution, however, the internal energy may deviate from its cold contribution; this happens when shocks form and we are no longer in the regime of thermodynamic equilibrium. We account for such processes by including a thermal pressure component

$$P_{\rm th} = (\Gamma_{\rm th}-1)(\epsilon-\epsilon_c)\,. \tag{3.13}$$

Note that in the static case, we have no equation for ϵ and instead rely entirely on the equation of state.

4 The field equations in spherical symmetry

From now on we assume spherical symmetry and write the line element in the form (3.3)

$$ds^2 = g_{\alpha\beta}dx^\alpha dx^\beta = -\alpha^2dt^2 + X^2dr^2 + \frac{r^2}{F}d\Omega^2\,,$$

It turns out convenient to write the two metric functions in terms of the variables

$$m = \frac{r}{2}\left(1-\frac{1}{FX^2}\right) \qquad \Leftrightarrow \qquad X^2 = \frac{1}{F}\left(1-\frac{2m}{r}\right)^{-1}\,, \tag{4.1}$$

$$\Phi = \ln(\sqrt{F}\alpha) \qquad \Leftrightarrow \qquad \alpha^2 = \frac{1}{F}e^{2\Phi}\,. \tag{4.2}$$

The metric functions are then determined by the field equations (2.2),

$$\partial_r\Phi = X^2F\left[\frac{m}{r^2} + 4\pi r\left(\bar{S}^r v + \frac{P}{F^2}\right) + \frac{r}{2F}(\eta^2+\psi^2)\right] - rFX^2W\,, \tag{4.3}$$

$$\partial_r m = 4\pi r^2(\bar{\tau}+\bar{D}) + r^2W + \frac{r^2}{2F}(\eta^2+\psi^2), \tag{4.4}$$

$$\partial_t m = r^2\frac{\alpha}{X}\left(\frac{1}{F}\eta\psi - 4\pi\bar{S}^r\right). \tag{4.5}$$

Note that (4.5) follows from the other two equations and is not required for obtaining m. As expected, the metric sector in spherical symmetry is completely determined by constraint equations. This does not hold for the scalar field which represents a dynamic degree of freedom and is determined by the wave equation (2.5) which we write in first-order form in terms of the Einstein scalar variable φ by defining

$$\eta = \frac{1}{X}\partial_r\varphi\,, \tag{4.6}$$

$$\psi = \frac{1}{\alpha}\partial_t\varphi\,. \tag{4.7}$$

With the identity $\partial_t\partial_r\eta = \partial_r\partial_t\eta$ we obtain

$$\partial_t\varphi = \alpha\,\psi\,, \tag{4.8}$$

$$\partial_t\eta = -\eta\frac{\partial_t X}{X} + \frac{\alpha}{X}\left(\partial_r\psi + \psi\frac{\partial_r\alpha}{\alpha}\right), \tag{4.9}$$

$$\partial_t\psi = \frac{\alpha}{X}\left[\partial_r\eta + \frac{2}{r}\eta + \eta\frac{\partial_r\alpha}{\alpha}\right] - \psi\frac{\partial_t X}{X} + 2\pi\alpha\left(\bar{\tau} - \bar{S}^r v + \bar{D} - 3\frac{P}{F^2}\right)F_{,\varphi} - \alpha F W_{,\varphi}\,. \tag{4.10}$$

Finally, the matter evolution is determined by out conserved set of partial differential equations

$$\partial_t\bar{D} + \frac{1}{\sqrt{F}r^2}\partial_r\left(r^2\frac{\alpha}{X}\sqrt{F}f_{\bar{D}}\right) = s_{\bar{D}}, \tag{4.11}$$

$$\partial_t\bar{S}^r + \frac{1}{r^2}\partial_r\left(r^2\frac{\alpha}{X}f_{\bar{S}^r}\right) = s_{\bar{S}^r}, \tag{4.12}$$

$$\partial_t\bar{\tau} + \frac{1}{r^2}\partial_r\left(r^2\frac{\alpha}{X}f_{\bar{\tau}}\right) = s_{\bar{\tau}}, \tag{4.13}$$

where

$$f_{\bar{D}} = \bar{D}v, \tag{4.14}$$

$$f_{\bar{S}^r} = \bar{S}^r v + \frac{P}{F^2}, \tag{4.15}$$

$$f_{\bar{\tau}} = \bar{S}^r - \bar{D}v, \tag{4.16}$$

$$s_{\bar{D}} = -\bar{D}\frac{F_{,\varphi}}{2F}\alpha\psi, \tag{4.17}$$

$$\begin{aligned} s_{\bar{S}^r} = {} & (\bar{S}^r v - \bar{\tau} - \bar{D})\alpha X F\left(8\pi r\frac{P}{F^2} + \frac{m}{r^2} - \frac{F_{,\varphi}}{2F^2X}\eta - rW\right) + \frac{\alpha X}{F}P\frac{m}{r^2} + 2\frac{\alpha P}{rXF^2} \\ & -r\alpha X\frac{PW}{F} - 2r\alpha X\bar{S}^r\eta\psi - \frac{3}{2}\alpha\frac{P}{F^2}\frac{F_{,\varphi}}{F}\eta - \frac{r}{2}\alpha X(\eta^2+\psi^2)\left(\bar{\tau} + \frac{P}{F^2} + \bar{D}\right)(1+v^2), \end{aligned} \tag{4.18}$$

$$s_{\bar{\tau}} = -\left(\bar{\tau} + \frac{P}{F^2} + \bar{D}\right)r\alpha X\left[(1+v^2)\eta\psi + v(\eta^2+\psi^2)\right] + \frac{\alpha}{2}\frac{F_{,\varphi}}{F}\left[\bar{D}v\eta + \left(\bar{S}^r v - \bar{\tau} + 3\frac{P}{F^2}\right)\psi\right] \tag{4.19}$$

Note that Eq. (4.11) can be cast in the alternative flux conservative form

$$\partial_t\bar{D} + \frac{1}{r^2}\partial_r\left(r^2\frac{\alpha}{X}f_{\bar{D}}\right) + \frac{F_{,\varphi}}{2F}\alpha\eta f_{\bar{D}} = s_{\bar{D}}\,, \tag{4.20}$$

5 The static limit

5.1 The equations in the static limit

The static limit is obtained by setting all time derivatives as well as the velocity v to zero. Because we do not need high-resolution shock capturing in the static case, we also write the equations in terms of the primitive matter variables. The result is

$$\partial_r \Phi = FX^2\left(\frac{m}{r^2}+4\pi r\frac{P}{F^2}+\frac{r}{2F}\eta^2\right)-rFX^2W\,, \tag{5.1}$$

$$\frac{\partial_r\alpha}{\alpha} = FX^2\left(\frac{m}{r^2}+4\pi r\frac{P}{F^2}+\frac{r}{2F}\eta^2\right)-\frac{F_\varphi}{2F}X\eta-rFX^2W\,, \tag{5.2}$$

$$\partial_r m = 4\pi r^2\frac{\rho h-P}{F^2}+\frac{r^2}{2F}\eta^2+r^2W\,, \tag{5.3}$$

$$\frac{\partial_r X}{X} = 4\pi rFX^2\frac{\rho h-P}{F^2}+\frac{r}{2}X^2\eta^2-FX^2\frac{m}{r^2}-\frac{F_{,\varphi}}{2F}X\eta+rFX^2W\,, \tag{5.4}$$

$$\partial_r P = -\rho hFX^2\left(\frac{m}{r^2}+4\pi r\frac{P}{F^2}+\frac{r}{2F}\eta^2-rW\right)+\rho h\frac{F_{,\varphi}}{2F}X\eta, \tag{5.5}$$

$$\partial_r\varphi = X\eta, \tag{5.6}$$

$$\partial_r\eta = -2\frac{\eta}{r}-2\pi X\frac{\rho h-4P}{F^2}F_{,\varphi}-F\eta X^2\frac{m}{r^2}-4\pi rX^2\eta\frac{P}{F}-\frac{r}{2}X^2\eta^3+\frac{X}{2}\frac{F_{,\varphi}}{F}\eta^2 + rFX^2W\eta+FXW_{,\varphi}\,. \tag{5.7}$$

A valuable diagnostic is provided by the baryon mass which is obtained from the baryon number density n_b and the mass per baryon m_b by

$$m_{\rm B} = m_b\int d^3x\sqrt{-g}n_bu^t = 4\pi\int_0^{r_s}dr\left\{r^2\frac{\rho}{F^{3/2}\sqrt{1-2m/r}}\right\}\,, \tag{5.8}$$

where we substituted $\rho = m_bn_b$. Finally, the gravitational mass can be calculated from quantities at the stellar surface by matching to an exterior solution. The result is given by Eq. (9) of [3] and translates into our notation as

$$m_{\rm grav} = r^2\partial_r\Phi_s\sqrt{1-\frac{2m}{r}}\exp\left\{-\frac{\partial_r\Phi_s}{\sqrt{(\partial_r\Phi_s)^2+X^2\eta^2}}\operatorname{arctanh}\left[\frac{\sqrt{(\partial_r\Phi_s)^2+X^2\eta^2}}{\partial_r\Phi_s+1/r}\right]\right\}. \tag{5.9}$$

This formula should not be necessary if the variable m is available at infinity as is the case in our static calculations. In that case, we may rescale our line element (3.3) to areal radius *in the Jordan frame*, i.e. set $r=\sqrt{F}\tilde{r}$, so that

$$ds^2 = -\alpha^2dt^2+X^2F\,d\tilde{r}^2+\tilde{r}^2d\Omega^2 = -\alpha^2dt^2+\left(1-\frac{2m}{r}\right)^{-1}d\tilde{r}^2+\tilde{r}^2d\Omega^2\,, \tag{5.10}$$

where we used the definition (4.1). We recover the spatial part of the Schwarzschild metric in this case and m evaluated at infinity is the ADM mass of the spacetime, i.e. the gravitational mass of Eq. (5.9). Numerically, this is indeed confirmed with high precision (about 1 part in 10^4 for standard resolutions).

For completeness, let us compare our equations with those of Ramazanoglu and Pretorius [11]. They work in the Einstein frame from the beginning and write the field equations (2.15)-(2.17) in the form

$$R_{\alpha\beta} = 8\pi T_{\alpha\beta} - 4\pi g_{\alpha\beta}T + 2\partial_\alpha\varphi\partial_\beta\varphi + m_\phi^2\varphi^2 g_{\alpha\beta}\,, \tag{5.11}$$

$$\Box\varphi = -4\pi\frac{a_{,\varphi}}{a}T + m_\phi^2\varphi\,. \tag{5.12}$$

We have checked that their version is indeed identical to ours if we set the potential

$$W(\varphi) = \frac{1}{2}M_\phi^2\varphi^2\,, \tag{5.13}$$

which is the expected expression for scalar field with particle mass M_φ.
Conformally rescaling the Jordan line element (3.3) to the Einstein frame gives us

$$d\bar{s}^2 = -F\alpha^2 dt^2 + FX^2 dr^2 + r^2(d\theta^2 + \sin^2\theta d\phi^2)\,, \tag{5.14}$$

which Ramazanoglu write as

$$ds^2 = -e^\nu dt^2 + \frac{dr^2}{\left(1-2\frac{\mu}{r}\right)} + r^2(d\theta^2 + \sin^2\theta d\phi^2)\,. \tag{5.15}$$

We thus identify the functions

$$\Phi = \frac{\nu}{2}\,, \qquad \mu = \frac{r}{2}\left(1 - \frac{1}{FX^2}\right) = m\,, \tag{5.16}$$

where $\Phi = \ln(\sqrt{F}\alpha)$ and m is our gravitational mass variable. We have verified that our Eqs. (5.1)-(5.7) are indeed equivalent to Eqs. (18) in [11] provided we relate their and our variables as summarized above. Note that they do not include the metric factors in their auxiliary derivative variable, so that they have $\Psi \equiv \partial_r\varphi$.

5.2 Compactification of the equation in the exterior

In order to impose boundary conditions at infinity, we need to switch to a compactified radial variable in the vacuum exterior. We therefore introduce $y := 1/r$, so that

$$\partial_r = -y^2\partial_y \qquad \Leftrightarrow \qquad \partial_y = -r^2\partial_r\,, \tag{5.17}$$

and change the variable $X\eta = \partial_r\varphi$ to $X\tilde{\eta} = \partial_y\varphi$ which implies

$$\eta = -y^2\tilde{\eta} \qquad \Leftrightarrow \qquad \tilde{\eta} = -r^2\eta\,. \tag{5.18}$$

The static equations (in vacuum) then become

$$\frac{\partial_y X}{X} = FX^2 m - \frac{1}{2}yX^2\tilde{\eta}^2 - \frac{1}{2}\frac{F_{,\varphi}}{F}X\tilde{\eta} - \frac{1}{y^3}FX^2W\,, \tag{5.19}$$

$$\partial_y\Phi = -FX^2 m - \frac{y}{2}X^2\tilde{\eta}^2 + \frac{1}{y^3}FX^2W\,, \tag{5.20}$$

$$\partial_y\varphi = X\tilde{\eta}\,, \tag{5.21}$$

$$\partial_y\tilde{\eta} = FX^2 m\tilde{\eta} + \frac{y}{2}X^2\tilde{\eta}^3 + \frac{1}{2}X\tilde{\eta}^2\frac{F_{,\varphi}}{F} - \frac{1}{y^3}FX^2\tilde{\eta}W + \frac{1}{y^4}FXW_{,\varphi}\,. \tag{5.22}$$

This form of the exterior equations, however, does not take into account the eponential Yukawa fall-off of the scalar field and the frequent divisions by y lead to divergencies in the numerical solution near infinity $y = 0$. In order to overcome this difficulty, we use the analytic knowledge about the asymptotic behaviour of the scalar field. Specifically, the field behaves as [11]

$$\lim_{r\to\infty} \varphi = A\frac{e^{-M_\varphi r}}{r} + B\frac{e^{M_\varphi r}}{r}\,. \tag{5.23}$$

We want to suppress the exponentially growing mode and therefore require $B = 0$ in the above equation. Numerically, we will enforce this by fixing $\varphi = 0$ at $y = 1/r = 0$. As mentioned, in combination with Eqs. (5.19)-(5.22), enforcing this boundary condition is not sufficient to suppress the exponentially growing mode. We therefore switch (following some testing) to the set of variables

$$\begin{aligned} \sigma &= \varphi e^{M_\varphi/y}\,, & \kappa &= -e^{M_\varphi/y}\eta = -e^{M_\varphi r}\eta\,, \\ \Leftrightarrow \quad \varphi &= \frac{\sigma}{e^{M_\varphi/y}}\,, & \eta &= -\frac{\kappa}{e^{M_\varphi/y}}\,. \end{aligned} \tag{5.24}$$

Furthermore, we find that using the mass variable m in place of X leads to less noise near $y = 0$. For changing from X to m, we note the relations

$$X = \frac{1}{\sqrt{F}}(1-2my)^{-1/2} \quad \Leftrightarrow \quad \frac{1}{FX^2} = 1-2my \quad \Leftrightarrow \quad m = \frac{1}{2y}\left(1-\frac{1}{FX^2}\right)\,. \tag{5.25}$$

For the numerical relaxation scheme, we also find the following relations useful,

$$\begin{aligned} \frac{\partial X}{\partial m} &= \frac{yX}{1-2my}\,, \\ \frac{\partial X}{\partial \sigma} &= -\frac{1}{2}X\frac{F_{,\sigma}}{F}\,, \\ \frac{\partial}{\partial m}\frac{1}{1-2y\,m} &= \frac{2y}{(1-2y\,m)^2}\,. \end{aligned} \tag{5.26}$$

The set of equations (5.19)-(5.22) then becomes

$$\partial_y m = -\frac{1}{2y^4 e^{2M/y}}\left(\frac{\kappa^2}{F} - M^2\sigma^2\right)\,, \tag{5.27}$$

$$\partial_y \Phi = -\frac{m}{1-2my} - \frac{1}{2(1-2my)y^3 e^{2M/y}}\left(\frac{\kappa^2}{F} - M^2\sigma^2\right)\,, \tag{5.28}$$

$$\partial_y \sigma = \frac{X\kappa - M\sigma}{y^2}\,, \tag{5.29}$$

$$\partial_y \kappa = -\kappa\partial_y\Phi + \frac{FXM^2\sigma + \kappa(2y-M)}{y^2} + \frac{X\kappa^2}{2y^2}\frac{F_{,\sigma}}{F}\,, \tag{5.30}$$

This set of differential equation is combined with the boundary conditions $FX^2 = 1$, $\Phi = 0$, $\eta = 0$ at the origin $r = 0$, $\rho = 0$ at the surface of the star as well as in the exterior, and $\varphi = 0$ at infinity $y = 0$.

6 Initial profiles

As in [5], we use two types of initial profiles, polytopic models and more realistic pre-supernova models.

(i) Polytrops: For these models, we solve the static limit of the field equations as summarized in the previous section. The equation of state is the same used in Sec. 3.3 of [5],

$$P = K\rho^\Gamma\,, \qquad \epsilon = \frac{K}{\Gamma-1}\rho^{\Gamma-1}\,,$$

$$\Gamma = \frac{4}{3}\,, \qquad K = 4.9345\times 10^{14}\ \ [\mathrm{cgs}]\,. \tag{6.1}$$

The central density and parameters of the conformal factor F are

$$\rho_c = 10^{10}\ \frac{\mathrm{g}}{\mathrm{cm}^3}\,, \tag{6.2}$$

$$\alpha_0 = 10^{-3}\,, \qquad \beta_0 = -20\,. \tag{6.3}$$

These models have very low density (in a relativistic sense) and therefore barely differ from the profile shown in Fig. 2 of Ref. [5]. Strong-field effects of the scalar field only emerge as nuclear densities are reached following the collapse.

(ii) Realistic SN progenitors: The second type of profiles used are obtained from Woosley and Heger [16] who evolve non-rotating single stars to the point of iron core collapse. So far, we have focused on their models with zero-age-main-sequence mass $M_{\rm ZAMS} = 12\ M_\odot$ and refer to this model henceforth as WH12. Like the polytropic model described above, the WH12 model is effectively a Newtonian star and we therefore initialize the scalar field as zero. For $\alpha_0 = 0$, a vanishing scalar field would also solve the time evolution equations and no scalar dynamics would emerge. We overcome this problem by using the small but non-zero $\alpha_0 = 10^{-3}$.

In practice, we use the polytopic model for testing the pointwise convergence properties of the code while the production runs and convergence analysis of the scalar wave signal at large radius are performed starting from the WH12 model.

7 Convergence analysis

We next study the convergence properties of the time evolution code. First, we consider the time evolution of the polytropic model described in the previous section. For this purpose, we follow the same procedure as in Sec. 4.2 of Ref. [5]. We employ a hybrid EOS with $\Gamma_1 = 1.3$, $\Gamma_2 = 2.5$ and $\Gamma_{\rm th} = 1.35$ while $K_1 = 4.9345\times 10^{14}$ [cgs] as predicted for a relativistic degenerate electron gas with fraction $Y_e = 0.5$ [15] and K_2 follows from continuity of the pressure across the matching density $\rho_{\rm nuc} = 2\times 10^{14}$ g cm^{-3}. The computational grid has uniform grid spacing in these simulations and extends to 2 000 km with $N_1 = 12\,000$, $N_2 = 18\,000$ and $N_3 = 24\,000$ points, respectively, for the low, medium and high resolution simulation. A grid variable f converges at $n^{\rm th}$ order if the differences between low, medium and high resolutions scale

$$\frac{f_{N_1} - f_{N_2}}{f_{N_2} - f_{N_3}} = Q_n := \frac{(N_2/N_1)^n - 1}{1-(N_2/N_3)^n}\,, \tag{7.1}$$

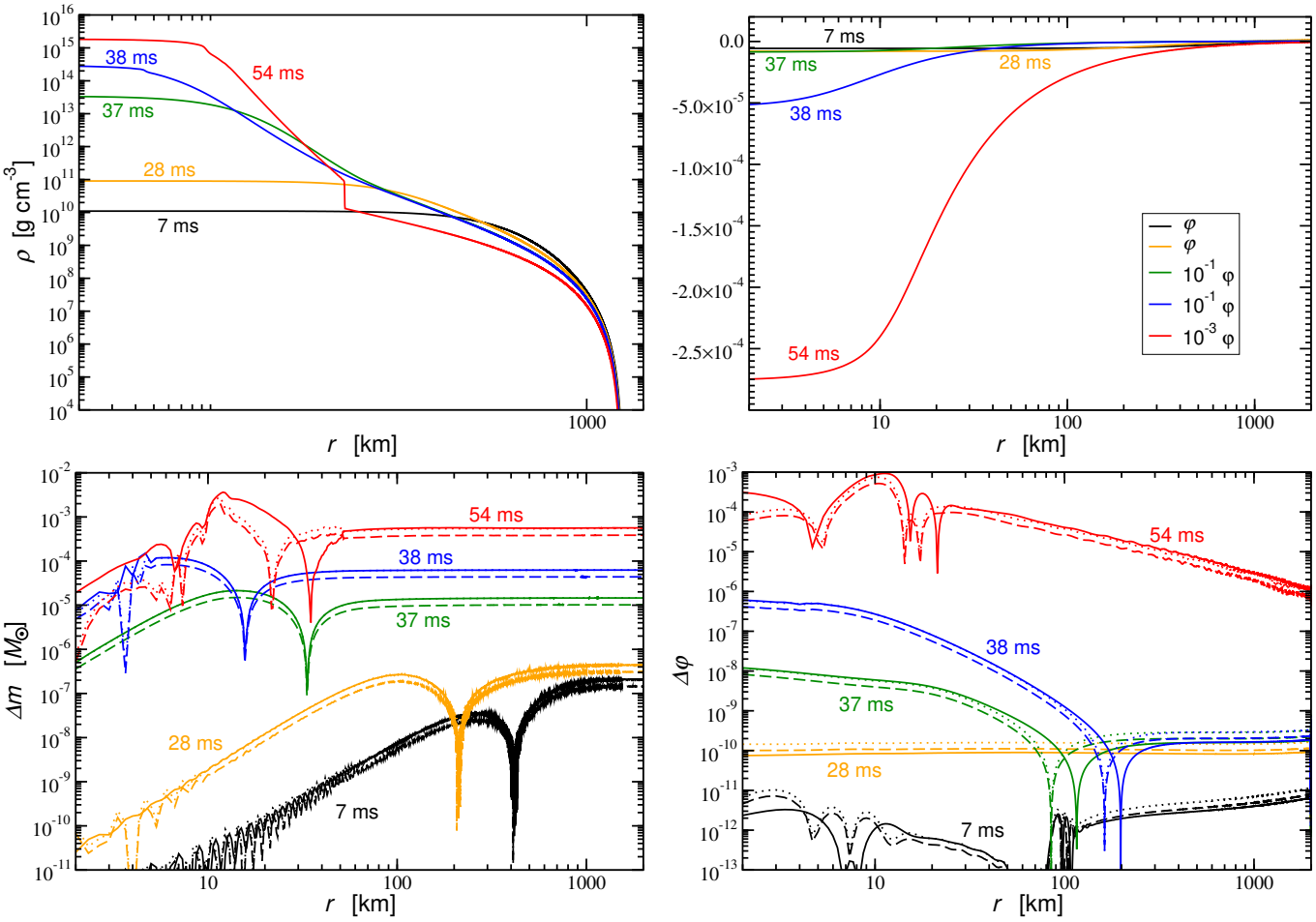

Figure 1: Convergence analysis for stellar collapse in massive ST theory. A polytropic initial profile collapses in a theory with $\alpha_0 = 10^{-3}$, $\beta_0 = -20$. Upper panels: Snapshots of the baryon density ρ (left) and the scalar field φ along the radius at different times of the evolution. For reference, core bounce occurs at 38 ms. Note that the scalar field at late times has been rescaled to allow for a comparison with the much smaller values at early times. Bottom panels: Difference in the mass function m (left) and the scalar field φ (right) obtained for N_1, N_2 and N_3 grid points. The solid curves show the differences obtained for N_1 and N_2 points. The dotted (dashed) curves are the difference for N_2 and N_3 points rescaled by the convergence factor $Q_2 = 2.86$ ($Q_1 = 2$) expected for second (first) order. If the solid line coincides with the dotted (dashed) curve, the code exhibits second (first) order convergence.

In Fig. 1, we display the differences $f_{N_1} - f_{N_2}$ as a function of radius at different times in the evolution as solid lines. The high-resolution difference $f_{N_2} - f_{N_3}$ is rescaled for second (first) order convergence using $Q_2 = 2.86$ ($Q_1 = 2$) as dotted (dashed) curves. If the solid line overlaps with the dotted (dashed) curve, the code exhibits second (first) order convergence. For reference, we also plot in the upper panels the profiles of the baryon density and the scalar field at the same moments in time. This figure is to be compared with Fig. 3 of [5] and shows very similar behaviour. Following the second-orderaccurate initialization of the profiles, boundary effects lead to a drop in convergence to

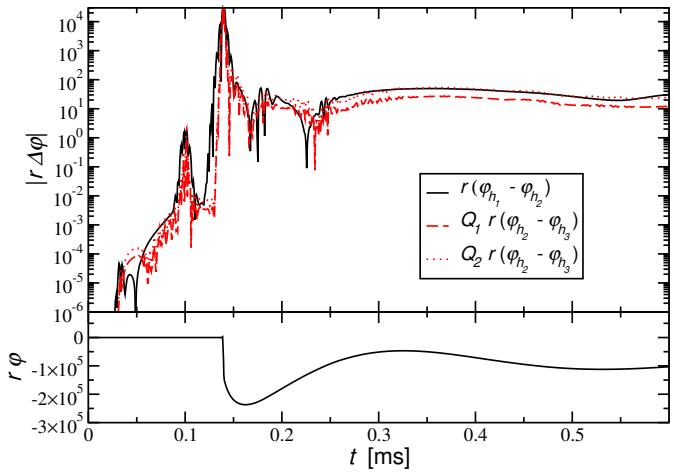

Figure 2: Convergence of the wave signal at $r = 30\,000$ km. As in Fig. 1, we have rescaled the high-resolution difference by the factor expected for second (first) order and compare the resulting dotted (dashed) curve with the low resolution difference shown as a solid curve. For oerientation, the smaller bottom panel shows the waveform $r\varphi$.

about first order after about one light crossing time $t \sim 7$ ms. As the dynamics picks up momentum, convergence is dominated by the smooth time evolution and approaches second order up to the core bounce at $t \sim 38$ ms when the first-order accurate shock capturing treatment sets in and the overall convergence properties result from a combination of first and second-order ingredients.
The pointwise convergence test requires us to employ a uniform grid while the production runs are performed with a non-uniform grid adapted to the high resolution requirements near the origin and the less demanding profiles propagating in the wave zone. In order to assess the accuracy of the waveforms generated, we have therefore performed a second convergence tests starting from the WH12 profile with the same EOS as in the first convergence study. The grid, however, is now of customized type using $N_1 = 5\,000$, $N_2 = 10\,000$ and $N_3 = 20\,000$ points on a grid uniformly spaced with $\Delta r_1 = 250$ m, $\Delta r_2 = 125$ m and $\Delta r_3 = 62.5$ m up to $r = 40$ km and the remainder of the grid points logarithmically spaced from that point on to the outer edge at $r_{\rm out} = 1.8 \times 10^5$ km. In contrast to the runs with a uniform grid, doubling the number of grid points does not lead to a decrease in the grid spacing by a factor 2 in the outer zone which complicates the convergence properties. We still expect the wave signal extracted at fixed radius (here $r_{\rm ex} = 3 \times 10^4$ km) to exhibit convergence similar to the first or second order behaviour seen above. As shown in Fig. 2, this is indeed the case. As before, we compare the low resolution differences with their high-resolution counterparts rescaled by $Q_1 = 2$ for first order (dashed curves) and $Q_2 = 4$ for second order. The figure shows that the gravitational waveform converges close to second order over most of the evolution. The error peaks at a retarded time of about $t - r_{\rm ex} \approx 140$ ms corresponding to the bounce stage in the stellar evolution where the wave signal shows a steep gradient (cf. lower panel in Fig. 2). Richardson extrapolation predicts an uncertainty for $N_2 = 10\,000$ points of about 3 % at bounce dropping to the percent level and below over the ensuing dynamics of the scalar field. We will use the 3 % as a conservative upper bound and use 10 000 for our production runs reported in the next section.

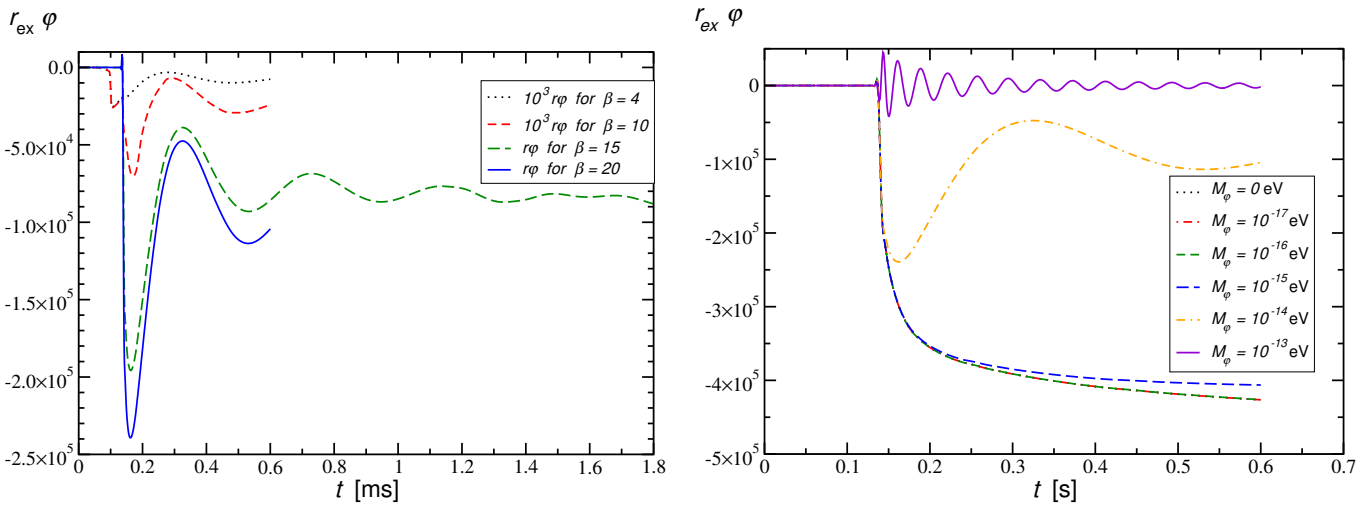

Figure 3: *Left panel:* The wave signal $r\varphi$ extracted at $r_{\rm ex} = 3 \times 10^4$ for various values of β_0 and fixed $\alpha_0 = 10^{-4}$, $M_\varphi = 10^{-14}$ eV. Note that we amplified the results for $\beta_0 = 4$ and $\beta_0 = 10$ by a factor 1000 to make their shape perceptible in comparison with the hugely scalarized cases $\beta_0 = 15$, 20. *Right panel:* $r\varphi$ for fixed $\alpha_0 = 10^{-4}$, $\beta_0 = 20$ for various values of the scalar mass parameter. Note that the curves for $M_\varphi = 0$, 10^{-17} eV and 10^{-16} eV lie on top of each other.

8 Extracted wave signals

[US: Most of the plots shown here have been done with `WHW02profile` set to 0 rather than 1 as needed. Tests for $\beta = -20$, $M_\varphi = 10^{-14}$ eV show that this does not change the results significantly, but we still need to redo the production runs. I also want to increase the resolution to 10 000 points to justify using the 3 % error determined in the previous section. Otherwise, the peak error is about 10 % which is larger than I would like. In any case, the plots shown here give a clear idea of what is happening.]
We now explore the parameter space of α_0, β_0 and M_φ to see the influence on the wave forms extracted at $r_{\rm ex} = 3 \times 10^4$ km. All simulations start with the WH12 profile, use 5 000 points on a custom grid with $\Delta r = 250$ m in the inner region and an outer radius of 1.8×10^5 km. The equation of state is always given by

$$\begin{aligned} \Gamma_1 &= 1.3\,, \\ \Gamma_2 &= 2.5\,, \\ \Gamma_{\rm th} &= 1.35\,, \\ K_1 &= 4.9345 \times 10^{14}\ [\text{cgs}]\,. \end{aligned} \tag{8.1}$$

The waveforms $r\varphi$ are shown for various parameter combinations in Fig. 3. From the left panel of the figure, we see that the degree of scalarization massively increases as we change β_0 from -10 to -15. In this regime we see *super scalarization*. The waveform not only reaches the values $|r\varphi| \sim 10^2 \ldots 10^3$ observed for the onset of strong scalarization in the collpase simulations in massless ST theory of [7, 9, 5] but exceeds these amplitudes by two to three orders of magnitude. As shown in the right panel, this is *not* a consequence of the mass term but the value of β_0: Even the massless case exhibits superscalarization which is nearly undistinguishable from low-mass scalar fields of $M_\varphi = 10^{-15} \ldots 10^{-17}$ eV. For larger M_φ, the amplitude drops to smaller though still enormous values. As

we will see in the next section, this is largely caused by the propagation of the scalar wave.
We also checked the impact on varying α_0 which is constrained to small values $\alpha_0 \lesssim 3.4 \times 10^{-3}$ by the Cassini space mission [2] [US: Do we know whether this bound and the other solar system tests are still valid for the mass range we consider?] . Tests we have performed so far vary α_0 from 10^{-4} to 3×10^{-4} and show no perceptible change in the waveforms. We need a few more runs, though, to strengthen this case.

9 Propagation of massive scalar signals

At large distances from the source, we assume that the propagation of the gravitational wave scalar is well approximated by the flat-space Klein-Gordon equation,

$$\partial_t^2\psi - \nabla^2\psi + m^2\psi = 0\,, \tag{9.1}$$

where $\nabla^2 = \partial_x^2+\partial_y^2+\partial_z^2$ in Cartesian coordinates. We have spherical symmetry, so that it is convenient to transform to spherical polar coordinates $\{r,\,\theta,\,\phi\}$, and ψ now depends only on r and t. Defining a new field $\sigma \equiv r\psi$, Eq.9.1 becomes a 1D wave equation for σ;

$$\partial_t^2\sigma - \partial_r^2\sigma + m^2\sigma = 0\,. \tag{9.2}$$

Let us consider a single mode, $\sigma \propto e^{-i(\omega t - kr)}$, plugging this into Eq. (9.2) gives the dispersion relation

$$\omega^2 = k^2 + m^2\,. \tag{9.3}$$

We obtain a real wavenumber (oscillatory solutions) for frequencies $\omega > m$, whereas for low-frequencies with $\omega < m$ the wavenumber is imaginary (exponential solutions). In particular, static potentials with $\omega = 0$ are exponentially damped giving the Yukawa potential. The phase velocity, $v_{\rm phase} = \omega/k = (1-(m^2/\omega^2))^{-1/2}$ is always greater than 1, whereas the group velocity, $v_{\rm group} = {\rm d}\omega/{\rm d}k = (1-(m^2/\omega^2))^{+1/2}$, is always less than 1.
In the massless case $v_{\rm group} = v_{\rm phase} = 1$, and the general solution to Eq.9.2 can be written as the sum of an ingoing and outgoing pulse which both propagate at the speed of light with no dispersion. This makes interpreting the output of core-collapse NR simulations particularly simple; one simply extracts the waveform from the signal at some radius r_1, this is called the extraction sphere, $\sigma(t;r_1) \equiv r_1\psi(t;r_1)$, the boundary conditions imposed are that this is purely outgoing so the signal observed by an observer at some larger radius r_2 is simply $\sigma(t-(r_2-r_1);r_2) = \sigma(t;r_1) \Rightarrow \psi(t-(r_2-r_1);r_2) = (r_1/r_2)\psi(t;r_1)$. We must ensure that r_1 is sufficiently large that the flat-space approximation in Eq. 9.1 holds. We now seek an analogous method to propagate signals out to large radii when $m \neq 0$. We have two ways of doing this which are described in the following sections.

9.1 Numerical evolution in the time domain

Given suitable initial data it is possible to numerically solve the partial differential equation in Eq. 9.2 using a 1+1 decomposition. This split can be implemented using the natural coordinates r and t. Alternatively, and much more efficiently, this split can be implemented using coordinates $u \equiv t - r$ and r. The coordinate u is the retarded time, and surfaces of constant u are null hypersurfaces, see Fig. 4.
ULI SHOULD DESCRIBE THE NUMERICAL METHOD, AND THE INITIAL DATA, HERE!
Given an initial signal on the extraction sphere, $\sigma(t;r_1)$, it is possible to numerically evolve this to obtain the signal at some larger radius, $\sigma(t;r_2)$.

9.2 Analytic evolution in the Fourier domain

In what follows we will use the following definitions for the Fourier transform,

$$\tilde{\sigma}(\omega,r) = \int_{-\infty}^{\infty} {\rm d}t\; \sigma(t,r_1)e^{i\omega t}\;,\;\; \text{and} \;\; \sigma(t,r) = \int_{-\infty}^{\infty} \frac{{\rm d}\omega}{2\pi}\; \tilde{\sigma}(\omega,r)e^{-i\omega t}\;. \tag{9.4}$$

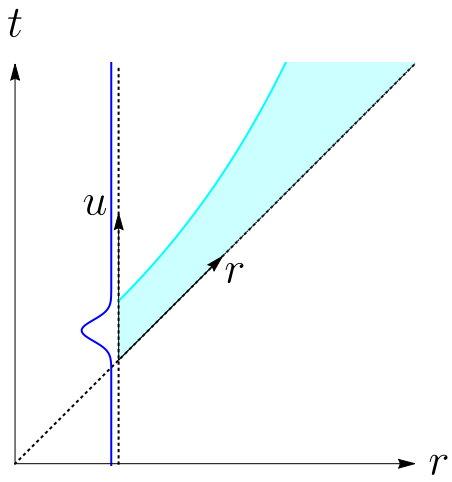

Figure 4: The diagram shows the standard r and t coordinates with solid lines and the $u = t - r$ and r coordinates in dotted lines. An initial pulse, illustrated in blue, propagates out with dispersion filling the shaded cyan region. It can be seen that a numerical grid in u and r can cover the cyan regions with far less "wasted space" than a grid using r and t.

Taking the Fourier transform of Eq. 9.2 gives the simple harmonic motion equation for $\tilde{\sigma}(\omega; r)$,

$$\partial_r^2 \tilde{\sigma}(\omega; r) = -(\omega^2 - m^2)\tilde{\sigma}(\omega; r) \ . \tag{9.5}$$

Defining $\chi \equiv +\sqrt{\omega^2 - m^2}$, the solution can be written in terms of two arbitrary functions of, $A(\omega)$ and $B(\omega)$,

$$\tilde{\sigma}(\omega; r) = A(\omega)\mathrm{e}^{\mathrm{i}\chi(r-r_1)} + B(\omega)\mathrm{e}^{-\mathrm{i}\chi(r-r_1)} \ , \tag{9.6}$$

$$\sigma(t; r) = \int \frac{\mathrm{d}\omega}{2\pi} \left(A(\omega)\mathrm{e}^{\mathrm{i}\chi(r-r_1)} + B(\omega)\mathrm{e}^{-\mathrm{i}\chi(r-r_1)} \right) \mathrm{e}^{-\mathrm{i}\omega t} \ . \tag{9.7}$$

We want to impose two physically motivated conditions on the otherwise arbitrary functions $A(\omega)$ and $B(\omega)$: (i) $\sigma(t; r)$ is real for all r, and (ii) $\tilde{\sigma}(\omega; r)$ decays faster that $1/r$ at large radii.

$$\text{(i)} \ \Rightarrow \ \tilde{\sigma}^*(\omega; r) = \tilde{\sigma}(-\omega; r)$$

$$\Rightarrow \begin{cases} A(\omega) = B^*(-\omega) & \text{for } \ |\omega| > m \\ A(\omega) = A^*(-\omega) \text{ and } \ B(\omega) = B^*(-\omega) & \text{for } \ |\omega| < m \end{cases}$$

$$\text{(ii)} \ \Rightarrow \ B(|\omega| < m) = 0$$

We can use conditions (i) and (ii) to eliminate $B(\omega)$ in favour of $A(\omega)$, and we also write the solution

as a integral over only positive frequencies;

$$\sigma(t;r) = \int_0^\infty \frac{\mathrm{d}\omega}{2\pi}\, A(\omega)\mathrm{e}^{\mathrm{i}\chi(r-r_1)}\mathrm{e}^{-\mathrm{i}\omega t} + B(-\omega)\mathrm{e}^{-\mathrm{i}\chi(r-r_1)}\mathrm{e}^{\mathrm{i}\omega t} + A(-\omega)\mathrm{e}^{\mathrm{i}\chi(r-r_1)}\mathrm{e}^{\mathrm{i}\omega t} + B(\omega)\mathrm{e}^{-\mathrm{i}\chi(r-r_1)}\mathrm{e}^{-\mathrm{i}\omega t}$$

$$\sigma(t;r) = \int_0^m \frac{\mathrm{d}\omega}{2\pi}\, \left(A(\omega)\mathrm{e}^{\mathrm{i}\chi(r-r_1)}\mathrm{e}^{-\mathrm{i}\omega t} + A(-\omega)\mathrm{e}^{\mathrm{i}\chi(r-r_1)}\mathrm{e}^{\mathrm{i}\omega t}\right) + \int_m^\infty \frac{\mathrm{d}\omega}{2\pi}\, \left(\left[A(\omega)\mathrm{e}^{\mathrm{i}\chi(r-r_1)}\mathrm{e}^{-\mathrm{i}\omega t} + A(-\omega)\mathrm{e}^{\mathrm{i}\chi(r-r_1)}\mathrm{e}^{\mathrm{i}\omega t}\right] + \text{c.c.}\right) . \tag{9.8}$$

From Eq. 9.8, and considering the sign of χ, it can be seen that $A(\omega > m)$ represent outgoing modes, $A(\omega < -m)$ represent ingoing modes, and $A(|\omega| < m)$ represent non-propagating modes (including the zero-frequency Yukawa term).

Imposing (i) and (ii) has removed one of the two free functions, it only remains to specify $A(\omega)$. To do this we impose boundary conditions on the NR extraction sphere at r_1; the conditions are (a) $\sigma(t;r_1) = \mathcal{N}(t) \;\Rightarrow\; \tilde{\sigma}(\omega;r_1) = \tilde{\mathcal{N}}(\omega)$ (since $\mathcal{N}(t)$ is real we have $\tilde{\mathcal{N}}^*(\omega) = \tilde{\mathcal{N}}(-\omega)$), and (b) $\sigma(t;r_1)$ contains no ingoing modes.

$$\text{(a) and (b)} \;\Rightarrow\; A(\omega) = \begin{Bmatrix} 0 & \text{for } \omega < -m \\ \tilde{N}(\omega) & \text{for } \omega > -m \end{Bmatrix} . \tag{9.9}$$

Substituting for $A(\omega)$ in Eq. 9.8 and returning to writing the solution as an integral over both positive and negative frequencies gives

$$\sigma(t;r) = \int_0^m \frac{\mathrm{d}\omega}{2\pi}\, \left(\tilde{\mathcal{N}}(\omega)\mathrm{e}^{\mathrm{i}\chi(r-r_1)}\mathrm{e}^{-\mathrm{i}\omega t} + \tilde{\mathcal{N}}(-\omega)\mathrm{e}^{\mathrm{i}\chi(r-r_1)}\mathrm{e}^{\mathrm{i}\omega t}\right) + \int_m^\infty \frac{\mathrm{d}\omega}{2\pi}\, \left(\tilde{\mathcal{N}}(\omega)\mathrm{e}^{\mathrm{i}\chi(r-r_1)}\mathrm{e}^{-\mathrm{i}\omega t} + \text{c.c.}\right) \tag{9.10}$$

$$\sigma(t;r) = \int_{-m}^m \frac{\mathrm{d}\omega}{2\pi}\, \tilde{\mathcal{N}}(\omega)\mathrm{e}^{\mathrm{i}\chi(r-r_1)}\mathrm{e}^{-\mathrm{i}\omega t} + \int_m^\infty \frac{\mathrm{d}\omega}{2\pi}\, \tilde{\mathcal{N}}(\omega)\mathrm{e}^{\mathrm{i}\chi(r-r_1)}\mathrm{e}^{-\mathrm{i}\omega t} + \int_{-\infty}^{-m} \frac{\mathrm{d}\omega}{2\pi}\, \tilde{\mathcal{N}}(\omega)\mathrm{e}^{-\mathrm{i}\chi(r-r_1)}\mathrm{e}^{-\mathrm{i}\omega t} \tag{9.11}$$

$$\sigma(t;r) = \int \frac{\mathrm{d}\omega}{2\pi}\, \tilde{\mathcal{N}}(\omega) \times \begin{Bmatrix} \mathrm{e}^{-\mathrm{i}\chi(r-r_1)} & \text{for } \omega < -m \\ \mathrm{e}^{+\mathrm{i}\chi(r_2-r_1)} & \text{for } \omega > -m \end{Bmatrix} \mathrm{e}^{-\mathrm{i}\omega t} \tag{9.12}$$

$$\boxed{\Rightarrow \tilde{\sigma}(\omega;r_2) = \tilde{\sigma}(\omega;r_1) \times \begin{Bmatrix} \mathrm{e}^{-\mathrm{i}\chi(r-r_1)} & \text{for } \omega < -m \\ \mathrm{e}^{+\mathrm{i}\chi(r_2-r_1)} & \text{for } \omega > -m \end{Bmatrix} .} \tag{9.13}$$

We now have a prescription for propagating massive signal with dispersion out to larger radii; firstly compute the Fouier transform of the initial data on the extraction sphere, then analytically propagate the Fourier domain signal using Eq. 9.13, and finally compute the inverse Fourier transform.

9.3 Comparing the two methods

As a test case we consider propagating a signal which, on the extraction sphere, is a simple cosine-Gaussian wavepacket,

$$\sigma(t;r_1) = \cos(\Omega t)\exp\left(\frac{-t^2}{2\varsigma^2}\right) . \tag{9.14}$$

We will choose $\Omega = 1/T$, $\varsigma = 30T$, and $m = 1/(15T)$, where T is an arbitrary time scale in the solution. We can approximate the solution to this simple case if we first notice that when $\Omega \gg 1/\varsigma$ the power spectrum of the initial data is localised to frequencies near $\omega = \pm\Omega$;

$$\tilde{\sigma}(\omega; r_1) = \sqrt{\frac{\pi}{2}}\varsigma\left(\exp\left(\frac{-\varsigma^2(\omega+\Omega)^2}{2}\right) + \exp\left(\frac{-\varsigma^2(\omega-\Omega)^2}{2}\right)\right). \tag{9.15}$$

This motivates expanding χ about the point $\omega = \Omega$ (we must have $\Omega \neq m$), which gives

$$\begin{aligned}\chi \equiv \sqrt{\omega^2 - m^2} &= \sqrt{\Omega^2 - m^2} + \frac{\Omega(\omega-\Omega)}{\sqrt{\Omega^2-m^2}} - \frac{m^2(\omega-\Omega)^2}{2(\Omega^2-m^2)^{3/2}} + \mathcal{O}\left((\omega-\Omega)^3\right) \\ &= \alpha + \beta(\omega-\Omega) + \gamma(\omega-\Omega)^3 .\end{aligned} \tag{9.16}$$

We can now find $\sigma(t; r_2)$ by taking the inverse Fourier transform of Eq. 9.13, using this approximation;

$$\begin{aligned}\sigma(t; r_2) \approx &\int_{-\infty}^{-m} \tfrac{\mathrm{d}\omega}{2\pi}\sqrt{\tfrac{\pi}{2}}\varsigma\left(\exp\left(\tfrac{-\varsigma^2(\omega+\Omega)^2}{2}\right)+\exp\left(\tfrac{-\varsigma^2(\omega-\Omega)^2}{2}\right)\right)\mathrm{e}^{-\mathrm{i}(r_2-r_1)(\alpha+\beta(\omega-\Omega)+\gamma(\omega-\Omega)^3)}\mathrm{e}^{-\mathrm{i}\omega t} \\ &+\int_{-m}^{\infty} \tfrac{\mathrm{d}\omega}{2\pi}\sqrt{\tfrac{\pi}{2}}\varsigma\left(\exp\left(\tfrac{-\varsigma^2(\omega+\Omega)^2}{2}\right)+\exp\left(\tfrac{-\varsigma^2(\omega-\Omega)^2}{2}\right)\right)\mathrm{e}^{\mathrm{i}(r_2-r_1)(\alpha+\beta(\omega-\Omega)+\gamma(\omega-\Omega)^3)}\mathrm{e}^{-\mathrm{i}\omega t}.\end{aligned} \tag{9.17}$$

In the limit $\Omega \gg 1/\varsigma$ this simplifies to

$$\sigma(t; r_2) \approx 2\Re\left\{\int_{-\infty}^{\infty}\frac{\mathrm{d}\omega}{2\pi}\sqrt{\frac{\pi}{2}}\varsigma\exp\left(\frac{-\varsigma^2(\omega-\Omega)^2}{2}\right)\mathrm{e}^{\mathrm{i}(r_2-r_1)(\alpha+\beta(\omega-\Omega)+\gamma(\omega-\Omega)^3)}\mathrm{e}^{-\mathrm{i}\omega t}\right\} \tag{9.18}$$

Everything in the exponential is now a quadratic form in ω, this is therefore a straightforward Gaussian integral which evaluates to

$$\sigma(t; r_2) \approx \Re\left(\frac{A\varsigma\exp\left(\frac{-\mathrm{i}\left(2\Delta m^2\left(\Delta\sqrt{\Omega^2-m^2}+t\Omega\right)+\sqrt{\Omega^2-m^2}\left(\Delta^2\Omega^2+2\Delta\sqrt{\Omega^2-m^2}\left(t\Omega+\mathrm{i}\varsigma^2\left(\Omega^2-m^2\right)\right)+t\left(\Omega^2-m^2\right)\left(t+2\mathrm{i}\varsigma^2\Omega\right)\right)\right)}{2\Delta m^2+2\mathrm{i}\varsigma^2(\Omega^2-m^2)^{3/2}}\right)}{\sqrt{\varsigma^2-\frac{\mathrm{i}\Delta m^2}{(\Omega^2-m^2)^{3/2}}}}\right) \tag{9.19}$$

where $\Delta = r_2 - r_1$. This approximation holds if $\Omega \gg 1/\varsigma$, as long as $\Omega \neq m$. Fig. 5 shows the excellent agreement between the two numerical methods of propagating a cosine-Gaussian pulse, and the analytic approximation in Eq. 9.19.

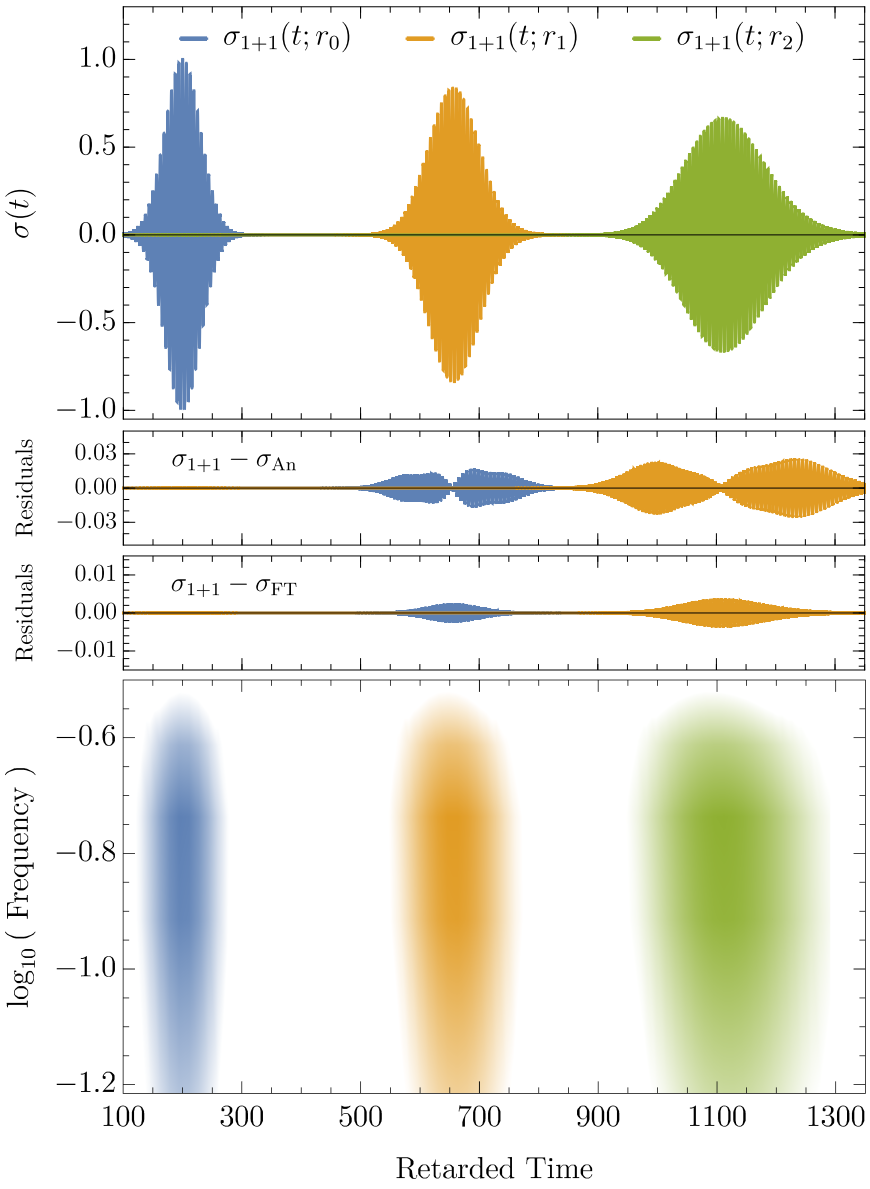

Figure 5: The top panel shows the behaviour of an initially cosine-Gaussian pulse as a function of retarded time, $u = t - r$, at three radii: the extraction radius r_0, $r_1 = r_0 + 204800T$, and $r_2 = 409600T$. The results in the top panel are computed by numerically integrating the wave equation as described in Sec. 9.1 (results obtained via this method are denoted $1+1$). The second panel shows the difference, or *residual*, between the $1+1$ method and the analytic approximation in Eq. 9.19 (the analytic approximation is denoted by subscript An). The residual between the $1+1$ and An results is less than $\sim 3\%$; this error set by the validity of the approximation $\Omega \gg 1/\varsigma$. The third panel shows the residual between the $1+1$ the Fourier transform method described in Sec. 9.2 (Fourier transform results are denoted by subscript FT). The agreement between $1+1$ and FT is better than $\sim 1\%$; this error is dominated by the grid resolution used in the $1+1$ numerical integration, the size of the residual scales with the resolution used. The bottom panel shows the spectogram of the data in the top panel. From either the top or bottom panel it can be seen that (i) the signal propagates slower than the speed of light (it propagates at speed $v_{\rm group}$), (ii) as the signal propagates it spreads out, and (iii) if you look carefully you can see that the high frequencies travel faster than the lower frequencies.

9.4 Asymptotic behavious of signals at large radii

Finally we wish to consider the limit of propagating a massive, dispersive signal a very large distance. This is obviously relevant to LIGO observing sources at astronomical distances. We will see that these dispersive signals almost "forget" the initial profile on the extraction sphere, and the signal at large distances tends to a generic "inverse" chirp. The large distance behaviour of a generic pulse is difficult to study using either of the methods presented above. The numerical 1+1 integration of the wave equation becomes prohibitively expensive when evolving forward large times; in the cosine-Gaussian example in Sec. 9.3 it took $\sim 1\,\text{day}$ to evolve the signal to r_2. The Fourier transform method is much better, but even this method suffers at extremely large astronomical distances of $> 1\,\text{kpc}$, this is because as the signal spreads out the length of the array needed to contain the signal grows without bound, therefore you end up having to take Fourier transforms of extremely large arrays and the computational memory available places an upper limit on the maximum distance out to which you can propagate a signal.

However, as the signals spread out the amplitude (or the envelope of the oscillating signal in Fig. 5) varies ever more slowly relative to the phase; in the limit of large distance the *stationary phase approximation* becomes an extremely good approximation. It should be noted that the stationary phase approximation becomes valid at large radii even if it was not valid for describing the initial waveform on the extraction sphere.

At large radii the frequencies with $|\omega| < m$ do not contribute because they decay exponentially with r. It wil be convinient to use the symmetry of the to write the signal as a integral over positive frequencies only;

$$\sigma(t;r_2) = 2\Re\left\{\int_m^\infty \frac{\mathrm{d}\omega}{2\pi}\, A(\omega)\mathrm{e}^{\mathrm{i}\Psi(\omega)}\mathrm{e}^{\mathrm{i}\sqrt{\omega^2-m^2}(r_2-r_1)}\mathrm{e}^{-\mathrm{i}\omega t}\right\} \equiv 2\Re\left\{\int_m^\infty \frac{\mathrm{d}\omega}{2\pi}\, A(\omega)\mathrm{e}^{\mathrm{i}\phi(\omega,t)}\right\}. \tag{9.20}$$

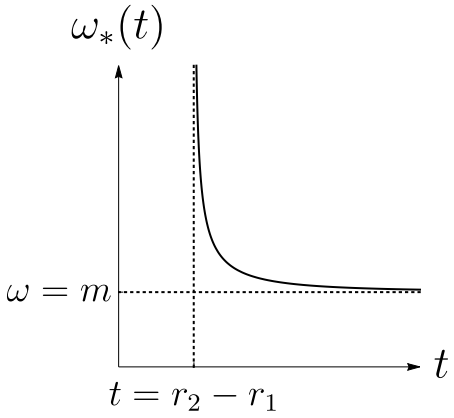

Figure 6: The time-frequency structure (see Eq. 9.23) of a pulse at large distances from the source. The frequency as a function of time, $\omega_*(t)$, follows an "inverse chirp"; before $t = r_2 - r_1$ no signal has arrived at r_2, the hig frequencies travel at nearly the speed of light and arrive shortly after $t = r_2 - r_1$, the low frequencies arrive later with frequencies near $\omega = m$ taking an infinitely long time to arrive. Frequencies $\omega < m$ are exponentially suppressed and never reach large radii.

At large radii the frequencies $|\omega| < m$ do not contribute because they decay exponentially with r. It will be convinient to use the conjugate symmetry between positive and negative frequencies to write

the $\sigma(t;r_2)$ as an integral over positive frequencies;

$$\sigma(t;r_2) = 2\Re\left\{\int_m^\infty \frac{\mathrm{d}\omega}{2\pi}\, A(\omega)\mathrm{e}^{\mathrm{i}\Psi(\omega)}\mathrm{e}^{\mathrm{i}\sqrt{\omega^2-m^2}(r_2-r_1)}\mathrm{e}^{-\mathrm{i}\omega t}\right\} \equiv 2\Re\left\{\int_m^\infty \frac{\mathrm{d}\omega}{2\pi}\, A(\omega)\mathrm{e}^{\mathrm{i}\phi(\omega,t)}\right\}, \qquad (9.21)$$

where $\phi(\omega,t) = \Psi(\omega) + \sqrt{\omega^2-m^2}(r_2-r_1) - \omega t$. The phase $\phi(\omega,t)$ has a stationary point when

$$\frac{\partial\phi(\omega,t)}{\partial\omega} = 0 \quad \Rightarrow \quad \Psi'(\omega) + \frac{\omega(r_2-r_1)}{\sqrt{\omega^2-m^2}} = t\,. \qquad (9.22)$$

Notice that the second term on the LHS can be written as $(r_2-r_1)/v_{\mathrm{group}}(\omega)$. In the limit $r_2 \gg r_1$ the $\Psi'(\omega)$ term can be neglected and Eq. 9.22 is solved by $\omega = \omega_*(t)$, with

$$\omega_*(t) = \frac{mt}{\sqrt{t^2-(r_2-r_1)^2}}\,. \qquad (9.23)$$

This gives the frequency of the observed signal at r_2 as a function of time; the frequency varies in an *inverse chirp* pattern (see Fig. 6) with low frequencies arriving later than high frequencies. The inverse chirp structure is easy to understand physically, the modes with a particular frequency arrive at the time that would be expected if they travelled at the group velocity at that frequency. We now calculate the amplitude as a function of time. The integrand in Eq. 9.21 is highly oscillatory when r_2-r_1 is large, except near the frequecy $\omega_*(t)$ which will dominate the result. Expanding the amplitude and the phase inside the exponential about this frequency we get

$$\sigma(t;r_2) = \Re\left\{2A(\omega_*)\mathrm{e}^{\mathrm{i}\phi(\omega_*)}\int_m^\infty \frac{\mathrm{d}\omega}{2\pi}\, \mathrm{e}^{\frac{\mathrm{i}}{2}(\omega-\omega_*)^2\frac{\mathrm{d}^2\phi}{\mathrm{d}\omega^2}\big|_{\omega=\omega_*}}\right\}. \qquad (9.24)$$

The integral in Eq. 9.27 is dominated by by frequencies near $\omega=\omega_*$, therefore at leading order in the approximation we are free to change the limits of integration provided the new range still contains ω_*;

$$\sigma(t;r_2) = \Re\left\{2A(\omega_*)\mathrm{e}^{\mathrm{i}\phi(\omega_*)}\int_0^\infty \frac{\mathrm{d}\omega}{2\pi}\, \mathrm{e}^{\frac{\mathrm{i}}{2}(\omega-\omega_*)^2\frac{\mathrm{d}^2\phi}{\mathrm{d}\omega^2}\big|_{\omega=\omega_*}}\right\}. \qquad (9.25)$$

This integral may be evaluated using a quater circle contour closed in the either the upper or lower half-plane depending on the sign of $(\mathrm{d}^2\phi/\mathrm{d}\omega^2)|_{\omega=\omega_*}$. This gives

$$\sigma(t;r_2) = \frac{A(\omega_*)(\omega_*-m^2)^{3/4}}{\sqrt{2\pi m^2(r_2-r_1)}}\Re\left\{\mathrm{e}^{\mathrm{i}\left[\Psi(\omega_*)-\omega_* t-\frac{\pi}{2}\right]}\right\}. \qquad (9.26)$$

$$\sigma(t;r_2) = \Re\left\{\frac{A(\omega_*)\mathrm{e}^{\Psi(\omega*)}\mathrm{e}^{\sqrt{\omega_*^2-m^2}(r_2-r_1)}\mathrm{e}^{-\mathrm{i}\omega_* t}}{\sqrt{\frac{\pi}{2}\left(\frac{r_2-r_1}{\sqrt{\omega_*^2-m^2}} - \frac{\omega_*^2\Delta}{(\omega_*^2-m^2)^{3/2}}\right)}}\right\}. \qquad (9.27)$$

$$\sigma(t;r_2) = \Re\left\{\frac{A(\omega_*)\mathrm{e}^{\mathrm{i}\Psi(\omega*)}\mathrm{e}^{\mathrm{i}\sqrt{\omega_*^2-m^2}(r_2-r_1)}\mathrm{e}^{-\mathrm{i}\omega_* t}}{\sqrt{\frac{\pi}{2}\frac{(r_2-r_1)m^2}{(\omega_*^2-m^2)^{3/2}}}}\right\}. \qquad (9.28)$$

This somewhat messy equation is actually really simple to interpret. The signal at any instant is almost monocromatic with frequency $\omega_*(t)$, this is the $\mathrm{e}^{-\mathrm{i}\omega_* t}$ term. There are several uninteresting phase terms, and instantaneous amplitude is given by $A(\omega_*)$, which depends on the initial data, divided by a factor which accounts for the stretching caused by the dispersion. To see why the denominator is related to the stretching it is helpful to note that the denominator of Eq. 9.27 can be written as $(\mathrm{d}/\mathrm{d}\omega)|_{\omega_*}((r_2-r_1)/v_{\mathrm{group}}(\omega))$; i.e. the rate of change of travel times for modes with a given frequency.

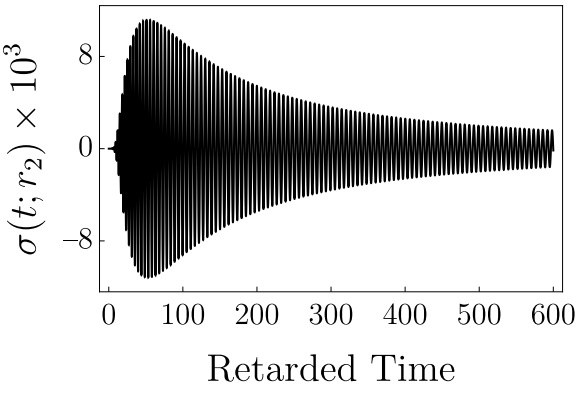

Figure 7: The asymptotic behaviour of an initially Gaussian pulse, $\sigma(t; r_1) = \exp(-t^2/(2\varsigma^2))$, after propagating a large distance. This was evaluated using Eq. 9.27 with $\varsigma = T$, $m = 1/T$, and $r_2 - r_1 = 100T$, where T is an arbitrary timescale.

10 The Klein-Gordon eq. in the stationary phase approximation

10.1 Preliminaries

The massive Klein-Gordon equation in 3+1D is given by

$$\partial_t^2\varphi - \nabla^2\varphi + m^2\varphi = 0\,. \tag{10.1}$$

In spherical coordinates, the Laplace operator is

$$\nabla^2 = \partial_r^2 + \frac{2}{r}\partial_r + \frac{1}{r^2\sin\theta}\partial_\theta\left(\sin\theta\,\partial_\theta\right) + \frac{1}{r^2\sin^2\theta}\partial_\phi^2\,, \tag{10.2}$$

so that in spherical symmetry, the 3+1D wave equation becomes

$$\partial_t^2\varphi - \partial_r^2\varphi - \frac{2}{r}\partial_r\varphi + m^2\varphi = 0\,. \tag{10.3}$$

By introducing $h := r\varphi$, we recover the 1+1D wave equation

$$\partial_t^2 h - \partial_r^2 h + m^2 h = 0\,. \tag{10.4}$$

Here m is the mass of the scalar particle; recall from Sec. 1.2 that $m = 10^{-15}\,\mathrm{eV}$ corresponds to a wavelength of about $2 \times 10^8\,\mathrm{m}$. The remainder of this section is devoted to studying the asymptotic behvaiour of solutions to this equation, specifically the behaviour of solutions at large times t.
We will employ for this purpose Fourier transforms relating functions in the spatial domain $f(x)$ to their transform $F(k)$ in the space of wave numbers. Even though it may appear surprising, it is indeed the use of the transform in the spatial sector that will give us ultimately the late-time behaviour of $h(t)$. We use the following convention for the Fourier transform,

$$\mathcal{F}[h](k) = \tilde{h}(k) = \int_{-\infty}^{\infty} h(x)e^{-ikx}dx\,, \tag{10.5}$$

$$\mathcal{F}^{-1}[\tilde{h}](x) = h(x) = \int_{-\infty}^{\infty} \tilde{h}(k)e^{ikx}dk\,. \tag{10.6}$$

The stationary phase approximation consists in evaluating integrals with a rapidly oscillating integrand by considering the dominant contribution near points where the phase in the oscillating factor is extremal. We follow here the notes [6] and start with the Fresnel integral

$$\int_{-\infty}^{\infty} e^{it^2/\varepsilon} dt = \sqrt{\frac{\pi}{2}|\varepsilon|}\,\left[1 + i\sigma(\epsilon)\right], \tag{10.7}$$

where $\sigma(\epsilon)$ denotes the sign of ϵ. Next, we consider the integral

$$I(\epsilon) := \int_{-\infty}^{\infty} A(t)\, e^{i\vartheta(t)/\epsilon} dt\,, \tag{10.8}$$

where $A : \mathbb{R} \to \mathbb{C}$ and $\vartheta : \mathbb{R} \to \mathbb{R}$ are smooth functions. In practice, we will often have A real valued, but do not impose this at this point. A stationary phase point is a point t_0 where $\vartheta'(t_0) = 0$ and we here also assume such points to be nondegenerate, i.e. $\vartheta''(t_0) \neq 0$.
Let us assume now that the integral (10.8) has exactly one stationary point. (If there are more, we simply add up the contributions of each.) Then for sufficiently small ϵ, the integral should be dominated by that part of the integrand near the stationary point. All other contributions are approximately cancelled due to the rapid oscillation of the $e^{i\vartheta(t)/\epsilon}$. The integral can therefore be approximated by Taylor expanding

$$\vartheta(t) = \vartheta(t_0) + \underbrace{\vartheta'(t_0)}_{=0}(t - t_0) + \frac{1}{2}\vartheta''(t_0)(t - t_0)^2 + \dots\,, \tag{10.9}$$

$$A(t) = A(t_0) + A'(t_0)(t - t_0) + \frac{1}{2}A''(t_0)(t - t_0)^2 + \dots\,. \tag{10.10}$$

In the stationary phase approximation, one typically keeps only the leading order term in the expansion of A while the linear term in the expansion of ϑ vanishes by construction and the quadratic term in the phase is evaluated using the result (10.7). To see this, we approximate (10.8) according to

$$\begin{aligned} I(\epsilon) &\approx \int_{-\infty}^{\infty} A(t_0) \exp\left\{\frac{i}{\epsilon}\left[\vartheta(t_0) + \frac{1}{2}\vartheta''(t_0)\,(t - t_0)^2\right]\right\} \\ &= A(t_0) e^{i\vartheta(t_0)/\epsilon} \int_{-\infty}^{\infty} \exp\left[\frac{i\vartheta''(t_0)}{2\epsilon} s^2\right] ds \end{aligned} \tag{10.11}$$

Comparing with (10.7), we see that $\varepsilon = 2\epsilon/\vartheta''(t_0)$, so that

$$\int_{-\infty}^{\infty} A(t)\, e^{i\vartheta(t)/\epsilon} dt \approx A(t_0) e^{i\vartheta(t_0)/\epsilon} \sqrt{\pi \left|\frac{\epsilon}{\vartheta''(t_0)}\right|}\left[1 + i\sigma\big(\frac{\epsilon}{\vartheta''(t_0)}\big)\right]. \tag{10.12}$$

It is this integral which we will return to in our analysis of the Klein-Gordon equation.

10.2 The Klein-Gordon equation

We write the Klein-Gordon equation (10.4) in the form $h_{tt} - h_{xx} + m^2 h = 0$ and Fourier transform this equation to obtain

$$\begin{aligned} & \mathcal{F}[h_{tt}] - \mathcal{F}[h_{xx}] + m^2 \mathcal{F}[h] = 0 \\ \Rightarrow \quad & \tilde{h}_{tt} + k^2 \tilde{h} + m^2 \tilde{h} = 0 \\ \Rightarrow \quad & \tilde{h}_{tt} = -(m^2 + k^2)\tilde{h} \\ \Rightarrow \quad & \tilde{h}(k,t) = \tilde{f}(k) e^{-i\omega(k)t} \,, \end{aligned} \tag{10.13}$$

where $\tilde{f}(k)$ can be regarded as the initial data and

$$\omega^2 = m^2 + k^2 \qquad \Leftrightarrow \qquad \omega = \pm\sqrt{m^2 + k^2} \,. \tag{10.14}$$

Since we have two solutions for ω, the solution (10.13) can be extended to the more general

$$\tilde{h}(k,t) = \tilde{f}(k) e^{-i\omega(k)t} + \tilde{g}(k) e^{i\omega(k)t} \,, \tag{10.15}$$

where we now keep ω strictly non-negative,

$$\omega = \sqrt{m^2 + k^2} \,. \tag{10.16}$$

We now require our signal in the time domain to be real which implies (noting $\omega(-k) = \omega(k)$)

$$\begin{aligned} & \tilde{h}(-k,t) = [\tilde{h}(k,t)]^* \\ \Rightarrow \quad & \tilde{f}(-k) e^{-i\omega(k)t} + \tilde{g}(-k) e^{i\omega(k)t} = [\tilde{f}(k)]^* e^{i\omega(k)t} + [\tilde{g}(k)]^* e^{-i\omega(k)t} \\ \Rightarrow \quad & \tilde{f}(-k) = [\tilde{g}(k)]^* \qquad \wedge \qquad \tilde{g}(-k) = [\tilde{f}(k)]^* \,. \end{aligned}$$

Applying the inverse Fourier transformation to (10.15) gives

$$\begin{aligned} 2\pi h(x,t) &= \int_{-\infty}^{\infty} \tilde{h}(k,t) e^{ikx} dk = \int_{-\infty}^{\infty} \tilde{f}(k) e^{ikx - i\omega(k)t} + \tilde{g}(k) e^{ikx + i\omega(k)t} \, dk \,, \\ 2\pi \dot{h}(x,t) &= \int_{-\infty}^{\infty} -i\omega(k) \, \tilde{f}(k) e^{ikx - i\omega(k)t} + i\omega(k) \tilde{g}(k) e^{ikx + i\omega(k)t} \, dk \end{aligned} \tag{10.17}$$

The goal is to study the late time behaviour of this solution, i.e. $h(x,t)$ for $t \to \infty$. It will be convenient to consider this behaviour along curves with fixed velocity $v := x/t$ which comes without loss of generality, as we will see. We then write (10.17) as

$$\begin{aligned} & 2\pi h(vt,t) = \int_{-\infty}^{\infty} \tilde{f}(k) e^{i\vartheta(k,v)t} + \tilde{g}(k) e^{i\theta(k,v)t} dk \qquad \text{with} \\ & 2\pi \dot{h}(vt,t) = \int_{-\infty}^{\infty} -i\omega(k) \, \tilde{f}(k) e^{i\vartheta(k,v)t} + i\omega(k) \, \tilde{g}(k) e^{i\theta(k,v)t} \, dk \,, \\ & \vartheta(k,v) = kv - \omega(k) \,, \qquad \theta(k,v) = kv + \omega(k) \,. \end{aligned} \tag{10.18}$$

We recognize the similarity with the integral on the left-hand side of Eq. (10.12) and thus apply the stationary phase approximation with smallness in ϵ now corresponding to a large t. We have two integrands here with one stationary phase point each. We calculate them as follows,

$$\begin{aligned}
\vartheta'(k) = 0 \qquad & \qquad \theta'(k) = 0 \\
\Rightarrow \quad v = \omega'(k) \qquad & \qquad \Rightarrow v = -\omega'(k) \\
\Rightarrow \quad v = \frac{k}{\sqrt{m^2+k^2}} \qquad & \qquad \Rightarrow v = -\frac{k}{\sqrt{m^2+k^2}} \\
\Rightarrow \quad k = \frac{mv}{\sqrt{1-v^2}} =: k_0 \qquad & \qquad \Rightarrow k = -\frac{mv}{\sqrt{1-v^2}} =: -k_0
\end{aligned} \tag{10.19}$$

Using these stationary points in (10.18), we obtain

$$\begin{aligned}
2\pi h(vt,t) &= \tilde{f}(k_0)e^{i\vartheta(k_0)t}\left[1+i\sigma\big(\vartheta''(k_0)\big)\right]\sqrt{\frac{2\pi}{|\vartheta''(k_0)|\,t}} \\
&\quad +\tilde{g}(-k_0)e^{i\theta(-k_0)t}\left[1+i\sigma\big(\theta''(-k_0)\big)\right]\sqrt{\frac{2\pi}{|\theta''(-k_0)|\,t}} \\
2\pi\dot{h}(vt,t) &= -i\omega(k_0)\,\tilde{f}(k_0)\,e^{i\vartheta(k_0)t}\,\left[1+i\sigma\big(\vartheta''(k_0)\big)\right]\sqrt{\frac{2\pi}{|\vartheta''(k_0)|t}} \\
&\quad +i\omega(k_0)\,\tilde{g}(k_0)\,e^{i\theta(-k_0)t}\,\left[1+i\sigma\big(\theta''(k_0)\big)\right]\sqrt{\frac{2\pi}{|\theta''(k_0)|t}}\,.
\end{aligned} \tag{10.20}$$

Using the definition of $\vartheta(k,v)$ and $\theta(k,v)$ in (10.18) together with $\Theta(-k_0) = -k_0 v + \omega(k_0) = -\vartheta(k_0)$, we find

$$\begin{aligned}
\vartheta'(k) = v - \frac{k}{\sqrt{m^2+k^2}} = -\vartheta'(-k) \qquad &\Rightarrow \qquad \vartheta''(k) = \frac{-m^2}{\sqrt{m^2+k^2}^3} = \vartheta''(-k)\,, \\
\theta'(k) = v + \frac{k}{\sqrt{m^2+k^2}} = -\theta'(-k) \qquad &\Rightarrow \qquad \theta''(k) = \frac{m^2}{\sqrt{m^2+k^2}^3} = \theta''(-k)\,,
\end{aligned} \tag{10.21}$$

we find $\theta''(-k_0) = -\vartheta''(k_0)$, so that their modulous in (10.20) is the same but their sign σ opposite. Finally recalling that $\tilde{g}(-k) = [\tilde{f}(k)]^*$ for real-valued signals in the time domain, we can simplify (10.20) to (recall $z + c.c. = 2\Re[z]$ and $-i(z - c.c.) = 2\Im[z]$)

$$\begin{aligned}
2\pi h(vt,t) &= 2\Re\left[\tilde{f}(k_0)e^{i\vartheta(k_0)t}(1-i)\sqrt{\frac{2\pi}{t}}\frac{1}{\sqrt{-\vartheta''(k_0)}}\right], \\
\frac{2\pi\dot{h}(vt,t)}{\omega(k_0)} &= 2\Im\left[\tilde{f}(k_0)e^{i\vartheta(k_0)t}(1-i)\sqrt{\frac{2\pi}{t}}\frac{1}{\sqrt{-\vartheta''(k_0)}}\right].
\end{aligned} \tag{10.22}$$

10.3 Practical application of the asymptotic solution

The problem with the result of the previous section is that we usually do not know the function $\tilde{f}(k_0)$. We may obtain it from the Fourier transform of the signal and it's derivative at $t = t_0$. Here, we pursue a different approach, however. We would like to know how a signal propagates from a large radius r_0 to another large radius r_1.

The only assumptions we make for this purpose are (i) that the stationary phase approximation is valid at r_1, (ii) that we know the signal $h(r_0, t)$ for all t, and (iii) that $\omega(r_0, t)$ is known and a smooth and monotonic function in t. In fact, we know that $\omega(r_0, t)$ is monotonically decreasing for a signal undergoing dispersion.

Our approach is to map the signal from the point (r_0, t_0) to the point (r_1, t_1). Note that the user specifies (r_0, t_0) and r_1, but not t_1. Instead, we know

$$\begin{aligned} & \omega_0 \coloneqq \omega(r_0, t_0) \\ \Rightarrow \quad & v = \sqrt{1 - \frac{m^2}{\omega_0^2}} \qquad \Rightarrow \qquad \frac{m^2}{\omega_0^2} = 1 - v^2 \\ \Rightarrow \quad & t_1 = t_0 + \frac{r_1 - r_0}{v} \,. \end{aligned} \tag{10.23}$$

From the second line, we also know that

$$\omega_0 = \frac{m}{\sqrt{1-v^2}} \,, \qquad k_0 = \frac{mv}{\sqrt{1-v^2}} \,. \tag{10.24}$$

Plugging this into (10.22), we obtain

$$\begin{aligned} h(r_1, t_1) &= \frac{1}{\pi} \Re \left[\tilde{f}(k_0) e^{im\sqrt{1-v^2}(t_1 - t_0)} \, (1-i) \sqrt{\frac{2\pi}{t_1 - t_0}} \frac{\sqrt{m}}{\sqrt{\sqrt{1-v^2}^3}} \right] \\ &= \frac{1}{\pi} \Re \left[\tilde{f}(k_0) \, (1-i) \, e^{-i\frac{m^2}{\omega_0}(t_1 - t_0)} \sqrt{\frac{2\pi}{t_1 - t_0}} \frac{\omega_0^{3/2}}{m} \right] \\ &= \frac{1}{\pi} \Re \left[\tilde{f}(k_0) \, (1-i) \, e^{-i\frac{m^2}{\sqrt{\omega_0^2 - m^2}}(r_1 - r_0)} \sqrt{\frac{2\pi\omega_0(\omega_0^2 - m^2)}{m(r_1 - r_0)}} \right] \\ \dot{h}(r_1, t_1) &= \frac{\omega_0}{\pi} \Im \left[\tilde{f}(k_0) \, (1-i) \, e^{-i\frac{m^2}{\sqrt{\omega_0^2 - m^2}}(r_1 - r_0)} \sqrt{\frac{2\pi\omega_0(\omega_0^2 - m^2)}{m(r_1 - r_0)}} \right] . \end{aligned} \tag{10.25}$$

It turns out convenient now to define

$$A_1 \coloneqq h(r_1, t_1) \,, \qquad B_1 \coloneqq \frac{\dot{h}(r_1, t_1)}{\omega_0} \,, \qquad \alpha \coloneqq \frac{m^2}{\sqrt{\omega_0^2 - m^2}} \,. \tag{10.26}$$

Our goal is to obtain the change in the signal as it propagates from some large r_1 to another $r_2 > r_1$. Again, we start with (r_0, t_0), and the proceed through Eqs. (10.23)-(10.25), merely with index $_1$

replaced with $_2$. Propagation of the signal from r_1 to r_2 then merely corresponds to a shift in time from t_1 to $t_2 + (r_2 - r_1)/\sqrt{1 - m^2/\omega_0^2}$ as well as a phase shift and rescaling of the signal given by

$$A_2 + iB_2 = (A_1 + iB_1)\, e^{-i\alpha(r_2 - r_1)} \sqrt{\frac{r_1 - r_0}{r_2 - r_0}} = \sqrt{\frac{r_1 - r_0}{r_2 - r_0}} (A_1 + iB_1)\, \{\cos[\alpha(r_2 - r_1)] - i \sin[\alpha(r_2 - r_1)]\}$$

$$\Rightarrow \quad h(r_2, t_2) = \sqrt{\frac{r_1 - r_0}{r_2 - r_0}}\, \{A \cos[\alpha(r_2 - r_1)] + B \sin[\alpha(r_2 - r_1)]\}$$

$$\Rightarrow \quad \boxed{h(r_2, t_2) = \sqrt{\frac{r_1 - r_0}{r_2 - r_0}} \left\{ h(r_1, t_1)\, \cos\left[\frac{m^2}{\sqrt{\omega_0^2 - m^2}}(r_2 - r_1)\right] + \frac{\dot{h}(r_1, t_1)}{\omega_0} \sin\left[\frac{m^2}{\sqrt{\omega_0^2 - m^2}}(r_2 - r_1)\right] \right\}} \tag{10.27}$$

Since the approximation relies on large r_1, r_2, we may set $r_0 = 0$ in the final equation.

11 Stationary phase reloaded

Upon closer reflection, Chris' calculation in the time domain has significant advantages over the spatial Fourier transformation I used in the previous section.

- Chris' expression enables us to propagate a signal from some radius to a larger one where only the larger radius needs to meet the requirements of the stationary phase approximation.
- The starting point of my approximation is the Fourier spectrum in space which involves two problems. First, in our core collapse simulations, at small radii, the equations to be solved are the full scalar-tensor theory plus matter equations and they are not approximated by the massive Klein-Gordon equation. Furthermore, the Fourier decomposition involves an integral over $x \in (-\infty, \infty)$ whereas in spherical symmetry, the spatial domain extends only over $r \in [0, \infty)$. Even if the latter could be overcome by some artificial extension of the spatial data from r to $-r$, it is not clear how to do this in a consistent manner.

Let us therefore apply the same ideas as in Sec. 10 but now to the case of Fourier transforming in time. This should give Chris' result provided both calculations are correct. So this is a check

11.1 The Klein Gordon equation

We want to solve the massive Klein-Gordon equation in one spatial dimension

$$\partial_t^2 \sigma - \partial_r^2 \sigma + m^2 \sigma = 0\,. \tag{11.1}$$

Let us use the same sign convention for the Fourier transform as in Chris' calculation,

$$\tilde{\sigma}(\omega, r) = \int_{-\infty}^{\infty} \sigma(t, r) e^{i\omega t}\, dt \qquad \Leftrightarrow \qquad \sigma(t, r) = \frac{1}{2\pi} \int_{-\infty}^{\infty} \tilde{\sigma}(\omega, r) e^{-i\omega t} d\omega\,. \tag{11.2}$$

Using $\mathcal{F}[\partial_t \sigma] = -i\omega\tilde{\sigma}$, we Fourier transform the Klein-Gordon equation (11.1) to

$$\partial_r^2 \tilde{\sigma}(\omega, r) = -(\omega^2 - m^2)\tilde{\sigma}(\omega, r)$$

$$\Rightarrow \quad \tilde{\sigma}(\omega, r) = \tilde{f}(\omega) e^{ik(\omega)\,(r - r_0)} + \tilde{g}(\omega) e^{-ik(\omega)\,(r - r_0)}\,, \tag{11.3}$$

where $k = \sqrt{\omega^2 - m^2}$. Note that k is the positive root here and that Chris calls this variable χ. The functions $\tilde{f}(\omega)$ and $\tilde{g}(\omega)$ are our initial conditions and setting $r = r_0$, we identify them with the Fourier transform $\tilde{\sigma}(\omega, r_0)$ of our waveform $\sigma(t, r_0)$ extracted at some radius r_0,

$$\tilde{\sigma}(\omega, r_0) = \tilde{f}(\omega) + \tilde{g}(\omega)\,. \tag{11.4}$$

Note that, unlike k, ω can be either positive or negative (or zero). Bearing in mind the signs in the exponents in Eq. (11.2) and the fact that $k(-\omega) = k(\omega)$, we see that for $\omega > m$, $\tilde{f}(\omega)$ and $\tilde{g}(-\omega)$ encode the outgoing signal, since then $\sigma(t, r) \sim e^{\pm i(kr - \omega t)}$. For $\omega < -m$, it is the other way round and for $-m < \omega < m$, $\tilde{g}$ leads to $\sigma(t, r) \sim e^{|k|\, r}$, i.e. diverges exponentially at large r, while $\tilde{f}(\omega)$ represents the exponentially decaying part $\sigma(t, r) \sim e^{-|k|\, r}$. (Note that ultimately we have only positive r; for $r \in (-\infty, \infty)$, bounded solutions would allow for neither $\tilde{f}$ nor $\tilde{g}$.) For $|\omega| = m$, we obtain a standing wave contribution $\sim [\tilde{g}(\pm m) + \tilde{f}(\pm m)]e^{\mp imt}$. We do not have such contributions at late or early times where we expect our signal to be zero and therefore assume $\tilde{f}(\mp m) = \tilde{g}(\pm m) = 0$ from now on. Our calculation largely works with $\tilde{f}$ and $\tilde{g}$ and therefore does not require us to distinguish between in and outgoing modes, but ultimately, we need to relate these two functions to our "initial" time domain signal $\sigma(t, r_0)$ and for that purpose, we must decide how $\tilde{\sigma}(\omega, r_0)$ is composed of in or outgoing parts. We assume it is purely outgoing in which case for positive frequencies

$$\boxed{\tilde{f}(\omega) = \tilde{\sigma}(\omega, r_0) \qquad \text{for } \omega \geq 0}\,. \tag{11.5}$$

It turns out that this is all we need to know about our initial data.
From our earlier discussion, we know that requiring the time domain signal to be real and bounded imposes the following conditions on $\tilde{f}$ and $\tilde{g}$:

$$\begin{aligned} &\text{for } |\omega| > m: && \tilde{g}^*(-\omega) = \tilde{f}(\omega) \quad \Leftrightarrow \quad \tilde{f}^*(-\omega) = \tilde{g}(\omega)\,, \\ &\text{for } |\omega| < m: && \tilde{g}(\omega) = 0 \quad \wedge \quad \tilde{f}^*(-\omega) = \tilde{f}(\omega)\,. \end{aligned} \tag{11.6}$$

11.2 Applying the stationary phase approximation

For arbitrary initial data, we can reconstruct the signal at radius r as a function of time t according to

$$\sigma(t, r) = \frac{1}{2\pi} \int_{-\infty}^{\infty} \left[\tilde{f}(\omega) e^{ik(r - r_0)} + \tilde{g}(\omega) e^{-ik(r - r_0)}\right] e^{-i\omega t}\, d\omega\,. \tag{11.7}$$

As before, we will consider the propagation of the signal along curves of constant velocity v and, for simplicity, we will set $r_0 = 0$ without loss of generality. We will bear in mind this shift in radius and eventually restore the r_0. We now have $r = vt$ and, thus,

$$\sigma(t, r) = \sigma(r/v, r) = \frac{1}{2\pi} \int_{-\infty}^{\infty} \left[\tilde{f}(\omega) e^{ikr} + \tilde{g}(\omega) e^{-ikr}\right] e^{-i\omega \frac{r}{v}} d\omega\,. \tag{11.8}$$

Let us define $\Sigma \coloneqq (-\infty, m] \cup [m, \infty)$ and $\bar{\Sigma} = (-m, m)$. Then

$$\begin{aligned}
\sigma(t,r) &= \frac{1}{2\pi}\int_{-\infty}^{\infty} \tilde{f}(\omega)e^{i\vartheta(\omega)r} + \tilde{g}(\omega)e^{i\theta(\omega)r}d\omega \\
&= \frac{1}{2\pi}\int_{\Sigma} \tilde{f}(\omega)e^{i\vartheta(\omega)r} + \tilde{g}(\omega)e^{i\theta(\omega)r}\,d\omega + \int_{\bar{\Sigma}} \tilde{f}(\omega)\underbrace{e^{-\sqrt{m^2-\omega^2}r}}_{\to 0} e^{-i\frac{\omega}{v}r}\,d\omega \\
&\approx \frac{1}{2\pi}\int_{\Sigma} \tilde{f}(\omega)e^{i\vartheta(\omega)r} + \tilde{g}(\omega)e^{i\theta(\omega)r}d\omega\,, \qquad (11.9)
\end{aligned}$$

with

$$\vartheta(\omega) = k - \frac{\omega}{v}\,, \qquad \theta(\omega) = -k - \frac{\omega}{v}\,, \qquad k = \sqrt{\omega^2 - m^2}\,. \qquad (11.10)$$

In the stationary phase approximation, this integral is dominated by contributions where $\vartheta'(\omega) = 0$ or $\theta'(\omega) = 0$, respectively. We can restore the integral range $(-\infty, \infty)$, therefore, by merely extending the functions $\vartheta(\omega)$ and $\theta(\omega)$ to the range $(-m, m)$ in a way such that they do not have vanishing derivatives in that range. The precise form of the extension does not affect the result in the stationary phase approximation as long as $\vartheta'(\omega) \neq 0 \neq \theta'(\omega)$ for $\omega \in (-m, m)$, so that we have got back to

$$\sigma(t,r) \approx \frac{1}{2\pi}\int_{-\infty}^{\infty} \tilde{f}(\omega)e^{i\vartheta(\omega)r} + \tilde{g}(\omega)e^{i\theta(\omega)r}d\omega\,. \qquad (11.11)$$

The rest is straightforward. We have

$$\begin{aligned}
&\vartheta'(\omega) = \frac{dk}{d\omega} - \frac{1}{v} = \frac{\omega}{\sqrt{\omega^2 - m^2}} - \frac{1}{v} \stackrel{!}{=} 0 \\
\Rightarrow\quad &v = v_{\mathrm{g}} = \frac{d\omega}{dk} = \sqrt{1 - \frac{m^2}{\omega^2}} \\
\Rightarrow\quad &\omega = \frac{m}{\sqrt{1-v^2}} =: \omega_0\,, \qquad k_0 \coloneqq k(\omega_0) = \sqrt{\omega_0^2 - m^2} = \frac{mv}{\sqrt{1-v^2}}\,, \qquad (11.12)
\end{aligned}$$

where we see that the propagation velocity v of the signal is given by the group velocity v_{g}. Note that $v > 0$ implies $\omega > 0$ and likewise for $v < 0$. This is in agreement with our earlier observation that $\tilde{f}(\omega)$ represents the outgoing contributions for positive and the ingoing ones for negative frequencies. A straightforward calculation gives

$$\vartheta'(\omega) = \frac{\omega}{\sqrt{\omega^2 - m^2}} - \frac{1}{v}\,, \qquad \theta'(\omega) = -\frac{\omega}{\sqrt{\omega^2 - m^2}} - \frac{1}{v}\,, \qquad \vartheta''(\omega) = -\theta''(\omega) = -\frac{m^2}{\sqrt{\omega^2 - m^2}^{\,3}}\,, \quad (11.13)$$

so that

$$\begin{aligned}
\vartheta(\omega_0) &= k_0 - \frac{\omega_0}{v} = \frac{mv}{\sqrt{1-v^2}} - \frac{m}{v\sqrt{1-v^2}} = -\sqrt{1-v^2}\frac{m}{v}\,, \qquad (11.14) \\
\vartheta''(\omega_0) &= -\frac{m^2}{\sqrt{\omega_0^2 - m^2}^{\,3}} = -\frac{\sqrt{1-v^2}^{\,3}}{mv^3} \quad \Rightarrow \quad \vartheta''(\omega_0) < 0 \quad \text{for all } \omega_0 \text{ with } 0 < v < 1\,.
\end{aligned}$$

We likewise obtain for the stationary phase of $\theta(\omega)$

$$\theta'(\omega) = -\frac{dk}{d\omega} - \frac{1}{v} = -\frac{\omega}{\sqrt{\omega^2 - m^2}} - \frac{1}{v} \stackrel{!}{=} 0 \tag{11.15}$$

$$\Rightarrow \quad v = -\frac{d\omega}{dk} = -\sqrt{1 - \frac{m^2}{\omega^2}} \qquad \Rightarrow \qquad \omega = -\omega_0 = -\frac{m}{\sqrt{1-v^2}}\,. \tag{11.16}$$

Note that now the frequency at which the phase is stationary is negative if the velocity is positive. Again, this is in agreement with our identification of $\tilde{g}(\omega)$ as representing the outgoing signal for negative frequencies. Note also that $k(-\omega_0) = k(\omega_0) = k_0$ does not change sign with ω. We have

$$\theta(-\omega_0) = -k_0 + \frac{\omega_0}{v} = \sqrt{1-v^2}\frac{m}{v} = -\vartheta(\omega_0) \tag{11.17}$$

$$\theta''(-\omega_0) = \frac{m^2}{\sqrt{\omega_0^2 - m^2}^{\,3}} = \frac{\sqrt{1-v^2}^{\,3}}{mv^3} \quad \Rightarrow \quad \theta''(-\omega_0) > 0 \quad \text{for all } \omega_0 \text{ with } 0 < v < 1\,.$$

In the stationary phase approximation, the signal in the time domain at radius r is therefore given by

$$\begin{aligned}
\sigma(t,r) &\approx \frac{1}{2\pi}\int_{-\infty}^{\infty} \tilde{f}(\omega_0) e^{i\left[\vartheta(\omega_0) + \frac{1}{2}\vartheta''(\omega_0)\,(\omega-\omega_0)^2\right]r} + \tilde{g}(-\omega_0) e^{i\left[\theta(-\omega_0) + \frac{1}{2}\theta''(-\omega_0)\,(\omega+\omega_0)^2\right]r}\, d\omega \\
&= \frac{1}{2\pi}\tilde{f}(\omega_0) e^{i\vartheta(\omega_0)r}\int_{-\infty}^{\infty} e^{i(\omega-\omega_0)^2/\varepsilon} d\omega + \frac{1}{2\pi}\tilde{g}(-\omega_0) e^{i\theta(-\omega_0)r}\int_{-\infty}^{\infty} e^{i(\omega+\omega_0)^2/\epsilon} d\omega\,,
\end{aligned} \tag{11.18}$$

where we set

$$\varepsilon := \frac{2}{\vartheta''(\omega_0)\, r}\,, \qquad\qquad \epsilon := \frac{2}{\theta''(-\omega_0)\, r} \stackrel{!}{=} -\varepsilon \tag{11.19}$$

Using the Fresnel integral

$$\int_{-\infty}^{\infty} e^{it^2/\varepsilon} dt = \sqrt{\frac{\pi}{2}|\varepsilon|}\;\left[1 + i\sigma(\epsilon)\right], \tag{11.20}$$

we find

$$\begin{aligned}
\sigma(t,r) &\approx \frac{1}{2\pi}\left[\tilde{f}(\omega_0) e^{i\vartheta(\omega_0)r}\sqrt{-\frac{\pi}{2}\varepsilon}\,(1-i) + \tilde{g}(-\omega_0) e^{i\theta(-\omega_0)r}\sqrt{\frac{\pi}{2}\epsilon}\,(1+i)\right] \\
&= \frac{1}{2\pi}\Big[\tilde{f}(\omega_0) e^{i\vartheta(\omega_0)r}\sqrt{-\frac{\pi}{2}\varepsilon}\,(1-i) + \underbrace{\tilde{g}(-\omega_0)}_{=\tilde{f}^*(\omega_0)} e^{-i\vartheta(\omega_0)r}\sqrt{\frac{\pi}{2}(-\varepsilon)}\,(1+i)\Big] \qquad (11.21) \\
&= \frac{1}{2\pi}\tilde{f}(\omega_0) e^{i\vartheta(\omega_0)r}\sqrt{-\frac{\pi}{2}\varepsilon}\,(1-i) + c.\,c. \qquad (11.22)
\end{aligned}$$

Finally substituting back for ε, $\vartheta(\omega_0)$ and $\vartheta''(\omega_0)$ and noting $z + c.\,c. = 2\Re[z]$, we get

$$\begin{aligned}
\sigma(r/v, r) &= \frac{1}{\pi}\Re\left[\tilde{f}(\omega_0) e^{-i\sqrt{1-v^2}mr/v}\sqrt{\frac{-\pi}{r\vartheta''(\omega_0)}}(1-i)\right] \qquad \Big|\; (1-i) = \sqrt{2}e^{-i\pi/4} \\
&= \sqrt{\frac{2mv^3}{\pi\sqrt{1-v^2}^{\,3}\, r}}\,\Re\left[\tilde{f}(\omega_0)\, e^{-i(m\sqrt{1-v^2}r/v + \pi/4)}\right] \qquad (11.23)
\end{aligned}$$

Now let us restore r_0 and compactify our notation by introducing/recalling

$$\boxed{\alpha := \frac{m(r-r_0)\sqrt{1-v^2}}{v}\,, \qquad \omega_0 = \frac{m}{\sqrt{1-v^2}}\,, \qquad v = \frac{r-r_0}{t}\,, \qquad k_0 = \frac{mv}{\sqrt{1-v^2}}}$$

$$\Rightarrow \quad \boxed{\sigma(t,r) = \frac{\sqrt{2}k_0}{\sqrt{\pi\alpha}}\,\Re\left[\tilde{f}(\omega_0)e^{-i(\alpha+\pi/4)}\right]}\,. \tag{11.24}$$

A less compact but physically intuitive way of writing this result makes use of the relation

$$k_0(r-r_0)-\omega_0 t = (k_0 v-\omega_0)t = \frac{mv^2-m}{\sqrt{1-v^2}}t = -m\sqrt{1-v^2} = -m\sqrt{1-v^2}\frac{r-r_0}{v} \overset{!}{=} -\alpha\,. \tag{11.25}$$

We then rewrite, also using that for outgoing initial data and positive frequencies $\tilde{f}(\omega_0) = \tilde{\sigma}(\omega_0, r_0)$,

$$\sigma(t,r) = \frac{\sqrt{2}k_0}{\sqrt{-\pi(k_0 v-\omega_0)t}}\,\Re\left[\tilde{\sigma}(\omega_0,r_0)e^{i(k_0 v-\omega_0)t}\,e^{-i\pi/4}\right]\,, \tag{11.26}$$

where we now take r_0 as the fixed original radius and r as the targeted (large) extraction radius. Time t varies and for each value of t, we have a velocity $v = (r-r_0)/t$ which, in turn, defines ω_0 and k_0. Then the term $k_0 v - \omega_0$ completely determines the dispersion: A diminishing of the amplitude $\propto 1/\sqrt{(k_0 v-\omega_0)t} = 1/\sqrt{(k_0 v-\omega_0)(r-r_0)/v}$ and a phase shift of the same magnitude. The overall phase shift $-\pi/4$ is a bit harder to understand. It seems to be associated as an overall shift acquired by the signal in the transition to the regime of validity of the stationary phase transition.
Finally, we would like to rewrite Eq. (11.26) in terms of amplitude $A(t)$ and phase $\phi(t)$, i.e. such that

$$\sigma(t,r) = A(t,r)\Re\left[e^{i\phi(t,r)}\right]\,. \tag{11.27}$$

This is achieved by writing

$$\tilde{\sigma}(\omega_0,r_0) = x+iy = \rho e^{i\varphi}\,, \tag{11.28}$$

whence

$$A(t,r) = \frac{\sqrt{2}k_0}{\sqrt{-\pi(k_0 v-\omega_0)t}}|\tilde{\sigma}(\omega,r)|\,, \qquad \phi(t,r) = \varphi(t)+(k_0 v-\omega_0)t-\frac{\pi}{4}\,,$$

$$|\tilde{\sigma}(\omega_0,r)| = \sqrt{x^2+y^2}\,, \qquad \varphi = \begin{cases} \arccos\frac{x}{\sqrt{x^2+y^2}} & \text{if } y\geq 0 \\ 2\pi-\arccos\frac{x}{\sqrt{x^2+y^2}} & \text{if } y<0\,, \end{cases} \tag{11.29}$$

and keeping track of integer multiples of 2π such that $\phi(t)$ is a continuous function.

References

[1] E. Berti, V. Cardoso, L. Gualtieri, M. Horbatsch, and U. Sperhake. Numerical simulations of single and binary black holes in scalar-tensor theories: circumventing the no-hair theorem. *Phys. Rev. D*, 87:124020, 2013. arXiv:1304.2836 [gr-qc].

[2] B. Bertotti, L. Iess, and P. Tortora. A test of general relativity using radio links with the Cassini spacecraft. *Nature*, 425:374–376, 2003.

[3] T. Damour and G. Esposito-Farèse. Nonperturbative strong field effects in tensor - scalar theories of gravitation. *Phys. Rev. Lett.*, 70:2220–2223, 1993.

[4] T. Damour and G. Esposito-Farése. Tensor - scalar gravity and binary pulsar experiments. *Phys. Rev. D*, 54:1474–1491, 1996.

[5] D. Gerosa, U. Sperhake, and C. D. Ott. Numerical simulations of stellar collapse in scalar-tensor theories of gravity. *Class. Quant. Grav.*, 33(13):135002, 2016.

[6] J. K. Hunter. Asymptotic expansion of integrals. Lecture notes.

[7] J. Novak. Neutron star transition to strong scalar field state in tensor scalar gravity. *Phys. Rev. D*, 58:064019, 1998.

[8] J. Novak. Spherical neutron star collapse toward a black hole in a tensor-scalar theory of gravity. *Phys. Rev. D*, 57:4789–4801, 1998.

[9] J. Novak and J. M. Ibáñez. Gravitational waves from the collapse and bounce of a stellar core in tensor scalar gravity. *Astrophys. J.*, 533:392–405, 2000.

[10] E. O'Connor and C. D. Ott. A New Open-Source Code for Spherically-Symmetric Stellar Collapse to Neutron Stars and Black Holes. *Class.Quant.Grav.*, 27:114103, 2010. arXiv:0912.2393 [astro-ph].

[11] F. M. Ramazanoglu and F. Pretorius. Spontaneous Scalarization with Massive Fields. *Phys. Rev. D*, 93(6):064005, 2016.

[12] J. S. Read, B. D. Lackey, B. J. Owen, and J. L. Friedman. Constraints on a phenomenologically parameterized neutron-star equation of state. *Phys. Rev. D*, 79:124032, 2009. arXiv:0812.2163 [astro-ph].

[13] M. Salgado. The cauchy problem of scalar-tensor theories of gravity. *Class. Quantum Grav.*, 23:4719–4741, 2006.

[14] M. Salgado, D. Martínez-del Río, M. Alcubierre, and D. Nuñez. Hyperbolicity of scalar-tensor theories of gravity. *Phys. Rev. D*, 77:104010, 2008.

[15] S. L. Shapiro and S. A. Teukolsky. *Black Holes, White Dwarfs, and Neutron Stars.* John Wiley & Sons, Inc., 1983.

[16] S. E. Woosley and A. Heger. Nucleosynthesis and Remnants in Massive Stars of Solar Metallicity. *Phys. Rept.*, 442:269–283, 2007. astro-ph/0702176.